

## **Response to Associate Editor Gerard Govers' comments**

Original AE comments are in *italicized text*.

Our replies are in plain text.

Bold text shows small corrections within the original text.

We (K. E. Clark and co-authors) are providing a revised version of our manuscript that has been granted publication subject to minor revisions by associate editor Gerard Govers. We would like to thank Dr. Govers for his careful consideration of our revised manuscript, and for his additional suggestions. We have now modified the manuscript in response to his comments, most notably addressing two issues: further discussing SOC mobilization in landslide depositional areas and clarifying the purpose of our calculation of landslide work. We provide detailed responses below to the areas that required authors' response. Our revised version incorporates these suggestions.

### **Detailed response to Gerard Govers' comments**

*My apologies that it took a while but I have now checked your revised manuscript. I would like to thank you for taking on board nearly all comments of the reviewers in a very profound manner and in my view the MS is now nearly ready for publication. I have added a few comments/questions in the attached draft, the most notable is related to Fig. 3c: could you check them and then submit your final version?*

We thank Dr. Govers for straightforward and positive comments on our paper. We address the comments/questions below in order as they appear in the manuscript, combining general and specific comments and numbering them one through eight.

#### **General and Specific comments:**

1) *Line 64: change erosioncarbon to erosion-carbon*

We thank the AE for bringing this typo to our attention and we have changed this in the text to read "erosion-carbon".

2) *Line 73: remove an "a" so the sentence should read as follows:*

"In this study, we mapped landslides in a mountainous catchment in the Andes of Peru over a 25-year period, including one year (2010) in which a large storm triggered numerous landslides."

3) *Line 74: Past tense would be more consistent ('mapped', quantified, assessed...)*

We have change quantify to quantified.

4) Line 87: describe San Pedro, with the suggestion was to say it is a village.

We have described San Pedro by including the following text:

“just downriver of San Pedro, **an area with an eco-lodge and one house and where the tributary San Pedro joins the Kosñipata River.**”

5) Line 152: GG proposes to add a version number and a trademark sign.

We have included the version number, but since Landsat and Quickbird would also require a trademark sign we have left this out from all instances. The new text reads as follows:

“The landslide inventory was produced by manually mapping landslide scars and their deposits in ArcGIS **using ArcMap 10.2.1**, and by verifying via ground-truthing of scars in the field.”

6) Line 165: *Would there also be a bias in your estimate of the amount of soil SOC mobilised? I do agree that all biomass will be mobilised both in the scar and the deposition area, but what about the soil OC. I would be tempted to state that, in the depositional area, this OC is not mobilised.*

We appreciate the AE’s comment. We have added discussion about this potential bias in the following text in Section 3.1:

“When considering the slope distribution of landslide areas, the deposit areas introduce some bias (see further discussion in Section 4.2, below). For the purposes of quantifying biomass disturbance and organic carbon fluxes associated with landslide activity, the convolution of scars and deposits is justified on the basis that all of these areas were covered in forest prior to landslide occurrence **and were then displaced during landslide failure**. However, the fate of **vegetation and soil** carbon from scars vs. deposits may differ, as discussed below. **Moreover, soil OC in low-slope depositional areas buried by landslide deposits may be less likely to erode than SOC not buried underneath landslides. Since this buried material is included in our calculation of the amount of SOC mobilized by landslides, we may to some extent overestimate landslide-associated SOC mobilization and the resulting amount of carbon accessible for fluvial transport.**”

7) Line 382: *In Section 4.2 GG suggests to remove the last part of this paragraph out:*

As suggested by GG, we have removed a sentence in Section 4.2 which deals with the potential implications for the relation between landslide occurrence and topography. We have removed the following text:

“However, our anecdotal field observations do not suggest that landslides at lower elevations have consistently longer run-out or larger deposit areas, so it is unlikely that such bias explains the observed relations between landslide occurrence and topography within our inventory”

The remaining text in this section of the manuscript now reads as follows:

“Since our mapping did not distinguish landslide scars from deposits (see Section 3.1), systematic changes in the ratio of scar to deposit area with elevation could influence apparent patterns of landslide occurrence **and landslide mobilised carbon**. For example, larger deposit areas at low elevation would increase calculated susceptibility even if the total landslide scar area were not larger, **though we have no direct evidence to suggest that this is the case.**”

*8) Line 473 in Section 5.1: I am not sure I fully get the reasoning behind this: what is it that you want to show here.*

We have expanded our discussion in this section of the text to clarify the purpose of our calculation of  $W$ , and we hope that this addresses the editor’s question:

“We can further explore the amount of work done, again in terms of landslide area, by the cumulative effect of repeated events of small magnitude versus occasional events of larger magnitude. **This analysis allows us to consider the relative importance of years with varying landslide area (cf. Wolman and Miller, 1960). In other words, does a year like 2010, characterized by very high landslide magnitude, occur often enough that these years dominate the long-term landslide record? Or do such years occur so rarely that, despite their high magnitude, they have little effect over the long term?** We calculate the % work done for a year with a given recurrence interval as  $W_i = (A_i/\Sigma A)/RI_i \times 100$ , where  $A_i$  is the landslide area in year  $i$  and  $\Sigma A$  is the total landslide area in the full dataset. **If  $W_i$  is high for a given year relative to other years, then this year is expected to have a disproportionately large effect on the long-term record, and vice versa. When our calculated  $W_i$  is plotted versus  $RI_i$  (Fig. 3c), we find that most years are characterized by a fairly similar value of  $W$ , with the exception of the most frequent years that are characterized by very little landslide activity (low  $RI$  and low  $W$ ). The relatively similar values of  $W$  despite large differences in landslide area (e.g., consider the very high  $SA$  in 2010) reflect the compensating effect of frequency and magnitude. Thus we expect that the long-term total landslide area resulting from years characterized by storm activity of varying magnitude is, on average, very similar in this setting. In other words, the landslide work done in years with rare, large storms is more or less similar to the sum of the total integrated work done in those years with smaller but more frequent storms.**”

1 **Storm-triggered landslides in the Peruvian Andes and implications for topography,**  
2 **carbon cycles, and biodiversity**

3 Kathryn E. Clark<sup>1\*</sup>, A. Joshua West<sup>2</sup>, Robert G. Hilton<sup>3</sup>, Gregory P. Asner<sup>4</sup>, Carlos A.  
4 Quesada<sup>5</sup>, Miles R. Silman<sup>6</sup>, Sassan S. Saatchi<sup>7</sup>, William Farfan-Rios<sup>6</sup>, Roberta E. Martin<sup>4</sup>,  
5 Aline B. Horwath<sup>8</sup>, Kate Halladay<sup>1</sup>, Mark New<sup>1,9</sup> and Yadvinder Malhi<sup>1</sup>

6 <sup>1</sup> Environmental Change Institute, School of Geography and the Environment, University of  
7 Oxford, Oxford, UK.

8 (\*correspondance: kathryn.clark23@gmail.com; Current address: Department of Earth and  
9 Environmental Science, University of Pennsylvania, Philadelphia, PA, USA)

10 <sup>2</sup> Department of Earth Sciences, University of Southern California, Los Angeles, CA, USA.

11 <sup>3</sup> Department of Geography, Durham University, Durham, UK.

12 <sup>4</sup> Department of Global Ecology, Carnegie Institution for Science, Stanford, CA, USA.

13 <sup>5</sup> Instituto Nacional de Pesquisas da Amazônia, Manaus, Brazil.

14 <sup>6</sup> Department of Biology and Center for Energy, Environment, and Sustainability, Wake  
15 Forest University, Winston-Salem, NC, USA.

16 <sup>7</sup> Jet Propulsion Laboratory, California Institute of Technology, Pasadena, CA, USA.

17 <sup>8</sup> Department of Plant Sciences, University of Cambridge, Cambridge, UK.

18 <sup>9</sup> African Climate and Development Initiative, University of Cape Town, Rondebosch, Cape  
19 Town, South Africa.

20 **Abstract**

21 In this study, we assess the geomorphic role of a rare, large-magnitude landslide-triggering event and  
22 consider its effect on mountain forest ecosystems and the erosion of organic carbon in an Andean  
23 river catchment. Proximal triggers such as large rain storms are known to cause large numbers of  
24 landslides, but the relative effects of such low-frequency, high-magnitude events are not well known  
25 in the context of more regular, smaller events. We develop a 25-year duration, annual-resolution  
26 landslide inventory by mapping landslide occurrence in the Kosñipata Valley, Peru, from 1988 to  
27 2012 using Landsat, Quickbird and Worldview satellite images. Catchment-wide landslide rates were  
28 high, at  $0.076\% \text{ yr}^{-1}$  by area. As a result, landslides on average completely turn over hillslopes every  
29  $\sim 1320$  years, although our data suggest that landslide occurrence varies spatially, such that turnover  
30 times are likely to be non-uniform. In total, landslides stripped  $26 \pm 4 \text{ tC km}^{-2} \text{ yr}^{-1}$  of organic carbon  
31 from soil (80%) and vegetation (20%) during the study period. A single rain storm in March 2010  
32 accounted for 27% of all landslide area observed during the 25-year study and accounted for 26% of  
33 the landslide-associated organic carbon flux. An approximately linear magnitude-frequency  
34 relationship for annual landslide areas suggests that large storms contribute an equivalent landslide  
35 failure area to the sum of smaller frequency landslides events occurring over the same period.  
36 However, the spatial distribution of landslides associated with the 2010 storm is distinct. On the basis  
37 of precipitation statistics and landscape morphology, we hypothesize that focusing of storm-triggered  
38 landslide erosion at lower elevations in the Kosñipata catchment may be characteristic of longer-term  
39 patterns. These patterns may have implications for the source and composition of sediments and  
40 organic material supplied to river systems of the Amazon basin, and, through focusing of regular  
41 ecological disturbance, for the species composition of forested ecosystems in the region.

## 42 1. Introduction

43 Landslides are major agents of topographic evolution (e.g., Li et al., 2014; Egholm et al., 2013;  
44 Ekström and Stark, 2013; Larsen and Montgomery, 2012; Roering et al., 2005; Hovius et al., 1997)  
45 and are increasingly recognized for their important biogeochemical and ecological role in  
46 mountainous environments because they drive erosion of carbon and nutrients (Pepin et al., 2013;  
47 Ramos Scharrón et al., 2012; Hilton et al., 2011; West et al., 2011; Stallard, 1985) and introduce  
48 regular cycles of disturbance to ecosystems (Restrepo et al., 2009; Bussmann et al., 2008). Landslides  
49 result when slope angles reach a failure threshold (Burbank et al., 1996; Schmidt and Montgomery,  
50 1995; Selby, 1993), which is thought to occur in mountains as rivers incise their channels, leaving  
51 steepened hillslopes (Montgomery, 2001; Gilbert, 1877). Landsliding acts to prevent progressive  
52 steepening beyond a critical failure angle for bedrock, even as rivers continue to cut downwards  
53 (Larsen and Montgomery, 2012; Montgomery and Brandon, 2002; Burbank et al., 1996). However,  
54 many slopes prone to landslide failure may remain stable until a proximal triggering event, such as a  
55 storm (Lin et al., 2008; Meunier et al., 2008; Restrepo et al., 2003; Densmore and Hovius, 2000) or a  
56 large earthquake (Li et al., 2014; Dadson et al., 2004; Keefer, 1994). Intense storms can increase pore  
57 pressure from heavy rainfall (Terzaghi, 1951), decreasing soil shear strength and resulting in slope  
58 failure (Wang and Sassa, 2003).

59 By clearing whole sections of forest and transporting materials downslope, landslides can drive fluxes  
60 of organic carbon from the biosphere (Hilton et al., 2011; West et al., 2011; Restrepo and Alvarez,  
61 2006), delivering the carbon either into sediments (where recently photosynthesized carbon can be  
62 locked away) or into the atmosphere, if ancient organic material in bedrock or soils is exposed and  
63 oxidized (Hilton et al., 2014). Links between storm frequency, landslide occurrence, and carbon  
64 fluxes could generate erosion-carbon cycle-climate feedbacks (West et al., 2011; Hilton et al., 2008a).  
65 Moreover, storm-triggered landslides may link climate to forest disturbance, with implications for  
66 ecosystem dynamics (Restrepo et al., 2009). However, for storm-triggered landslides to keep  
67 occurring over prolonged periods of time, hillslopes must remain sufficiently steep, which typically  
68 occurs in mountains via sustained river incision. Incision is also climatically regulated (Ferrier et al.,  
69 2013), providing a mechanism connecting storm activity, erosion, and topographic evolution (e.g.,  
70 Bilderback et al., 2015), and further linking to organic carbon removal from hillslopes and ecological  
71 processes across landscapes.

72 In this study, we mapped landslides in a mountainous catchment in the Andes of Peru over a 25-year  
73 period, including one year (2010) in which a large storm triggered a numerous landslides. We  
74 quantified landslide rates on an annual basis and use comprehensive datasets on soil and above- and  
75 below-ground biomass to determine the amount of organic carbon stripped from hillslopes. We assess  
76 the relative landslide ‘work,’ in terms of total landslide area, done in different years to explore the

77 roles of varying magnitudes and frequencies of triggering events, providing a longer-term context for  
78 understanding storm-triggered landslides that has not been available in much of the prior research on  
79 storm effects. We also evaluate the spatial distribution of landslides with respect to catchment  
80 topography and climatic factors that may act as potential longer-term forcing on the location of most  
81 active landslide erosion. Finally, we assess the potential role of these spatial patterns in shaping  
82 regional topography, determining the composition of sediment delivered to rivers, and influencing  
83 forest ecosystems that are repeatedly disturbed by landslide occurrence.

84

## 85 2. Study area

86 The Kosñipata River (Fig. 1) is situated in the Eastern Andes of Peru. We focus on the catchment area  
87 upstream of a point (13°3'27"S 71°32'40"W) just downriver of San Pedro, an area with an eco-lodge  
88 and one house and where the tributary San Pedro joins the Kosñipata River. Elevation in the  
89 catchment ranges from 1200 metres above sea level (m) to 4000 m, with a mean elevation ( $\pm 1$   
90 standard deviation) of  $2700 \pm 600$  m and a catchment area of  $185 \text{ km}^2$ . The forested area covers  $150$   
91  $\text{km}^2$  and consists of tropical montane cloud forest at high elevations and sub-montane tropical  
92 rainforest at lower elevations (Fig. 1a) (Horwath, 2011). The area of puna grasslands covers  $35 \text{ km}^2$   
93 above the timberline at  $3300 \pm 250$  m range. The valley is partially contained in Manu National Park,  
94 where logging is prohibited. A single unpaved road is located in the valley stretching from high to low  
95 elevations. The Kosñipata River flows through the study area and into the Alto Madre de Dios River,  
96 which feeds the Madre de Dios River, a tributary of the Amazon River. There are extensive datasets  
97 on plants, soil, ecosystem productivity, carbon and nutrient cycling and climate within the catchment  
98 (Malhi et al., 2010). Tree species richness ranges from 40 to 180 species  $\text{ha}^{-1}$  for trees  $\geq 10$ cm diameter  
99 at breast height (dbh), and total forest C-stocks (Gurdak et al., 2014; Girardin et al., 2013; Horwath,  
100 2011; Gibbon et al., 2010) are representative of the wider Andean region (Saatchi et al., 2011).

101 The South American Low Level Jet carries humid winds westward over the Amazon Basin and then  
102 south along the flank of the Andes, driving orographic rainfall in the Eastern Cordillera of the Central  
103 Andes (Espinoza et al., 2015; Lowman and Barros, 2014; Marengo et al., 2004). In the study area,  
104 precipitation ranges from 2000 to 5000  $\text{mm yr}^{-1}$  and is highest at the lowest elevations, decreasing  
105 approximately linearly with the increase in elevation (Clark et al., 2014; Girardin et al., 2014b;  
106 Huaraca Huasco et al., 2014). Much of the valley has  $>75\%$  cloud cover throughout the year in a band  
107 of persistent cloud that spans much of the Eastern Andes, although cloud immersion is restricted to  
108 elevations  $> \sim 1600$  m (Halladay et al., 2012) (Fig. 1a).

109 The Kosñipata Valley is in the tectonically active setting of the uplifting Eastern Cordillera of the  
110 Central Andes, associated with subduction of the Nazca Plate under the South American Plate

111 (Gregory-Wodzicki, 2000). Since 1978, there have been ~4 registered earthquakes larger than  
112 magnitude  $M=5$  within a distance of 65 km from the Kosñipata Valley (Fig. 1b; USGS, 2013a;  
113 Gregory-Wodzicki, 2000), though significant ground shaking within the Kosñipata Valley has not  
114 been reported during the study interval. The Cusco fault zone is the nearest seismically active region,  
115 ~50 km southwest of the study site, consisting of normal faults stretching 200 km long and 15 km  
116 wide parallel to the Andean plateau (Cabrera et al., 1991) and where deep earthquakes are common  
117 (USGS, 2013a; Tavera and Buforn, 2001). In the Andean foothills, ~20 km northeast of the study site,  
118 there is an active fold and thrust belt (Vargas Vilchez and Hipolito Romero, 1998; Sébrier et al.,  
119 1985). The bedrock geology in the Kosñipata Valley is representative of the wider Eastern Andes  
120 (Clark et al., 2013). The catchment is dominated by metamorphosed sedimentary rocks in the high  
121 elevations (mostly mudstone protoliths of ~450 Ma) and a plutonic region in the lower elevations  
122 (Carlotto Caillaux et al., 1996; Fig. 1b).

123 Landslides are a pervasive feature of the landscape in the Kosñipata Valley. In general in the Andes,  
124 landslides are a common geomorphic process, with landslide area covering 1-6% of mountain  
125 catchments in parts of Ecuador and Bolivia (Blodgett and Isacks, 2007; Stoyan, 2000), and landslide-  
126 associated denudation rates have been estimated in the range of  $9\pm 5$  mm yr<sup>-1</sup> (Blodgett and Isacks,  
127 2007). Downstream of the Kosñipata River, detrital cosmogenic nuclide concentrations in river  
128 sediments in the Madre de Dios River suggest a denudation rate of ~0.3 mm yr<sup>-1</sup> (Wittmann et al.,  
129 2009), although this catchment includes a large lowland floodplain area. Cosmogenic-derived total  
130 denudation rates in the high Bolivian Andes range up to ~1.3 mm yr<sup>-1</sup> (Safran et al., 2005) and  
131 suspended sediment derived erosion rates up to 1.2 mm yr<sup>-1</sup> (Pepin et al., 2013). The difference  
132 between the landslide-associated erosion rates measured in Bolivia (Blodgett and Isacks, 2007) and  
133 the catchment-averaged denudation rates typical of this region has not been widely considered, and a  
134 more systematic comparison including data paired from identical catchments could offer fruitful  
135 avenues for further investigation. For purposes of this study, the observation of relatively high  
136 landslide rates suggests at the least that landslides are the primary mechanism of hillslope mass  
137 removal, as they are in other active mountain belts (Hovius et al., 2000; Hovius et al., 1997).

138

### 139 **3. Materials and methods**

#### 140 **3.1. Landslide mapping**

141 Landslides within the Kosñipata Valley were manually mapped over a 25-year period from 1988 to  
142 2012 using Landsat 5 (Landsat Thematic Mapper) and Landsat 7 (Landsat Enhanced Thematic  
143 Mapper Plus) satellite images (Fig. 2a) (USGS, 2013b). There were 38 usable Landsat images for the  
144 region over the 25-year period, with 1-3 available for each year (see Supplement Table S1). All  
145 images were acquired in the dry season (May-October). Landsat images were processed with a

146 Standard Terrain Correction (Level 1T) which consists of systematic radiometric and geometric  
147 processing using ground control points and a digital elevation model (DEM) for ortho-georectification  
148 (USGS, 2013b). The high frequency of the Landsat images made it possible to develop a time series  
149 of individual landslides over the entire 25-year duration which has not typically been achieved before  
150 in studies at the catchment-scale (Hilton et al., 2011; Hovius et al., 1997).

151 The landslide inventory was produced by manually mapping landslide scars and their deposits in  
152 ArcGIS [using ArcMap 10.2.1](#), and by verifying via ground-truthing of scars in the field. Mapping  
153 involved visually comparing images from one year to the next evaluating contrasting colour changes  
154 suggesting a landslide had occurred. A composite image of Landsat bands 5 (near-infrared, 1.55-1.75  
155  $\mu\text{m}$ ), 3 (visible red, 0.63-0.69  $\mu\text{m}$ ) and 7 (mid-infrared, 2.08-2.35  $\mu\text{m}$ ) was used in order to identify  
156 landslide scars with the greatest spectral difference to forest. Bedrock outcrops are minimal in the  
157 valley and thus not subject to mislabelling as landslides. Several aerial photographs (from 1963 and  
158 1985) were used to identify and remove pre-1988 landslides from this study.

159 The landslide areas visible via spectral contrast in the Landsat images include regions of failure, run-  
160 out areas, and deposits. In some of the high-resolution imagery, we were able to distinguish scars  
161 from deposits, but not systematically enough to separately categorize these for the full landslide  
162 catalogue in this study. One 2007 landslide was coupled to a particularly large debris flow and stood  
163 out within our inventory, with the 1.7 km long debris flow comprising ~5% of the total landslide area  
164 for the total inventory from 1988 to 2012. With this one exception, we consider all areas with visible  
165 contrast outside of river channels as being “landslide” area (e.g., see Fig. 2a and inset photo). [When](#)  
166 [considering the slope distribution of landslide areas, the deposit areas introduce some bias](#)  
167 [\(see further discussion in Section 4.2, below\)](#). For the purposes of quantifying biomass  
168 disturbance and organic carbon fluxes associated with landslide activity, the convolution of scars and  
169 deposits is justified on the basis that all of these areas were covered in forest prior to landslide  
170 occurrence [and were then displaced during landslide failure](#). However, the fate of [vegetation and soil](#)  
171 carbon from scars vs. deposits may differ, as discussed below. [Moreover, soil OC in low-slope](#)  
172 [depositional areas buried by landslide deposits may be less likely to erode than SOC not buried](#)  
173 [underneath landslides. Since this buried material is included in our calculation of the amount of SOC](#)  
174 [mobilised by landslides, we may to some extent overestimate landslide-associated SOC mobilisation](#)  
175 [and the resulting amount of carbon accessible for fluvial transport](#). Future landslide mapping work,  
176 taking advantage of even higher resolution imagery than available in this study, would benefit from  
177 the effort to explicitly distinguish scars and deposits for full inventories.

178 The Landsat images had a mean visibility of 67% that varied year-to-year (Table S2; Fig. 3a). Non-  
179 visible portions were due to topographic shadow, cloud shadow, and no-data strips on Landsat 7  
180 images post-2002 (following failure of the satellite’s scan line corrector). Duplicate or triplicate

181 images were used in most years, and so landslides obscured by cloud shadow or no-data were likely to  
182 be spotted within a year of their occurrence. Topographic shadow produced by hillslopes covered a  
183 minimum of 21% of the study area (35 km<sup>2</sup> out of 185 km<sup>2</sup>), predominantly on southwest facing  
184 slopes (223±52° azimuth), and was consistently present between images. Landslides that fell within  
185 these shadow areas were not visible. Using Quickbird imagery from 2005 (which covers 54% of the  
186 study area) we found that the Landsat topographic shadow areas have a similar area covered by  
187 landslides as the visible areas; 26% of the Quickbird-mapped landslide area fell within Landsat  
188 topographic shadow areas, and these areas encompass a similar 22% of the total image area. We thus  
189 infer that landslide occurrence under Landsat topographic shadow is approximately equivalent to that  
190 in the visible portion of the Landsat images. On this basis, we estimate an error of < ~20% in our  
191 landslide inventory due to missed landslides under topographic shadow.

192 Small-area landslides are not fully accounted for by our mapping approach due to the Landsat grid-  
193 resolution of 30 m x 30 m (Stark and Hovius, 2001). In addition, Landsat images may not allow  
194 distinguishing of clumped landslides (cf. Marc and Hovius, 2015; Li et al., 2014). We assessed the  
195 potential bias by comparing the Landsat imagery with Quickbird imagery from 2005 (at 2.4 m x 2.4 m  
196 resolution). Specifically, we compared landslides mapped from portions of 2005 Quickbird image that  
197 are visible in the Landsat imagery (i.e., not in topographic shadow, discussed above) with the  
198 Landsat-derived landslides mapped from 1988 to 2005 that had not recovered by 2005. The difference  
199 in landslide area is 181,760 m<sup>2</sup>, equivalent to ~25% of the total landslide area. The area-frequency  
200 relationships (cf. Malamud et al., 2004 and references therein) for the two datasets show similar  
201 power law relationships for large landslides (Fig. 4) and illustrate that the different total landslide  
202 areas can be attributed mainly to missing small landslides (< 4,000 m<sup>2</sup>) in the Landsat-derived maps.  
203 These small landslides contribute ~80% of the observed difference, with the remaining difference  
204 attributable to 3 larger landslides (total area 30,500 m<sup>2</sup>) missed due to other reasons such as image  
205 quality. Based on the difference between total landslide area mapped via Quickbird vs. Landsat  
206 imagery, we estimate an error of ~20% in our landslide inventory from missing small landslides and  
207 <5% error from missing larger landslides.

### 208 **3.2 Landslide rates, turnover times, and landslide susceptibility**

209 We calculated landslide rate ( $R_{ls}$ , % yr<sup>-1</sup>) as the percentage of landslide area ( $A_{ls}$ ) per unit catchment  
210 area ( $A_{catchment}$ ), i.e.,  $R_{ls} = 100 \times A_{ls}/A_{catchment} \times 1/25$  yr for all landslide area observed during the 25-  
211 year study period. To assess the spatial distribution of landslides throughout the study area, we  
212 determined rates by 1 km<sup>2</sup> grid cells (Fig. 2b).

213 The average rate of slope turnover due to landslides ( $t_s$ ) is the inverse of landslide rate. This metric  
214 reflects the time required for landslides to impact all of the landscape, solely based on their rate of

215 occurrence (Hilton et al., 2011; Restrepo et al., 2009).  $t_{is}$  was quantified over the visible portion of the  
216 study area in 1 km<sup>2</sup> cells (Fig. 2c).

217 To assess how landslide rate varies with elevation and hillslope angle, we divided each landslide  
218 polygon into 3 m x 3 m cells consistent with the Carnegie Airborne Observatory (CAO) digital  
219 elevation model (DEM) (Asner et al., 2012; see Appendix A). We used the resulting 3 m grid to  
220 calculate histograms of landslide areas and total catchment area as a function elevation and slope  
221 using 300 m and 1° intervals, respectively (Figs. 5, 6). We also defined landslide susceptibility ( $S_{ls}$ )  
222 for a given range of elevation or slope angle values, as the ratio of the number of landslide cells in  
223 each elevation (or slope) range, divided by the total number of catchment cells in the equivalent  
224 range. Consistent with the landslide rate analysis, we only used catchment cells in the portion of the  
225 study area visible in the Landsat images.

### 226 **3.3. Calculation of carbon stripped from hillslopes by landslides**

#### 227 **3.3.1. General approach to calculating landslide-associated carbon fluxes**

228 We seek to quantify the amount of organic carbon mobilised by landslides at the catchment scale.  
229 This requires knowledge of the spatial distribution of carbon stocks on forested hillslopes at this scale.  
230 One approach is to use forest inventory maps derived from field surveys, aerial imagery, or other  
231 remote sensing observations (Asner et al., 2010; Saatchi et al., 2007) along with mapped landslides  
232 (e.g., Ramos Scharrón et al., 2012; West et al., 2011). However, such forest inventories do not  
233 typically capture below-ground or soil carbon stocks, the latter of which can make up the majority of  
234 total organic carbon in the landscape (Eswaran et al., 1993). Maps of soil C can be estimated from soil  
235 surveys together with knowledge of the C content in each soil type (Ramos Scharrón et al., 2012), but  
236 sufficiently detailed soil surveys are often unavailable and it is also difficult to test the key assumption  
237 that C content is constant for a given soil type.

238 An alternative approach, which we adopt in this study, is to use empirical trends in C stocks as a  
239 function of elevation, and to assign landslide area at a given elevation with a C stock value  
240 representative of that elevation (Hilton et al., 2011). Scatter in the relationship between elevation and  
241 C stocks (cf. Fig. 7, Table 1) means these trends do not provide the basis for a robust map of C stocks,  
242 nor a precise value for any single individual landslide. However, landslides in a setting like the  
243 Kosñipata Valley occur distributed across the catchment area at a given elevation, and the large  
244 number of landslides effectively samples from the observed scatter in C stocks. This averaging means  
245 that, when we sum together estimates of C stock stripped by all landslides across the catchment, we  
246 can estimate a representative mean value for the total flux of landslide-associated carbon. An implicit  
247 assumption is that there is not a systematic, coincident spatial bias in both landslide location and C  
248 stock at a given elevation (e.g., see discussion of potential slope biases on C stock estimates, below).

### 249 3.3.2. Carbon stocks as a function of elevation

250 To constrain trends in C stocks with elevation in the Kosñipata catchment, we collated soil and  
251 vegetation datasets, taking advantage of the numerous plot studies. The datasets consist of soil carbon  
252 stocks, above ground living biomass (trees), and root carbon stocks (Girardin et al., 2010). Each  
253 dataset consisted of data from 6 to 13 plots along the altitudinal gradient (Fig. 7). Linear regressions  
254 of C stock ( $\text{tC km}^{-2}$ ) versus elevation (m) were determined for the soil, above ground living biomass,  
255 and roots separately (Hilton et al., 2011) and are reported in Table 1. For above ground living  
256 biomass, we assumed a wood carbon concentration of 46% measured in stems and leaves ( $n = 130$ )  
257 throughout the Kosñipata Valley (Rao, 2011). The trend in above ground biomass versus elevation  
258 from this dataset fits within the range reported by Asner et al. (2014). Additionally, data on wood  
259 debris carbon stocks (Gurdak et al., 2014), and epiphyte carbon stocks (Horwath, 2011) are available  
260 but were not used in the carbon stock analysis because: (i) these comprise a small proportion of the  
261 total biomass (see below), and (ii) do not show systematic change with elevation, precluding the use  
262 of our elevation-based approach for these biomass components.

263 For soil organic carbon (SOC) stocks, we used data from soil pits along the altitudinal gradient. Pits  
264 were dug at 11 forest plots, each with 6 to 51 individual soil pits per plot. Soil pits were dug from the  
265 surface at 0.05 to 0.5 m depth intervals until reaching bedrock, which was typically found at  $\sim 1$  m  
266 depth (see Supplement Table S3). Carbon stocks were determined by multiplying interval depth (m)  
267 and measured soil organic carbon content (%OC) by bulk density ( $\text{g cm}^{-3}$ ) for each soil layer. %OC  
268 was measured at each layer for every pit. For each plot one pit was measured for bulk density at the  
269 following intervals: 0-5, 5-10, 10-20, 20-30, 30-50, 50-100, 100-150 cm, and the depth-density trend  
270 from this pit was applied to other pits from the same plot. Soils were collected and processed  
271 following the methods Quesada et al. (2010). An average SOC stock (in  $\text{tC km}^{-2}$ ) for each plot was  
272 determined from the mean of individual pit SOC stocks (Fig. 7a; Table S3).

273 Compared to previously published SOC data for this region, this dataset is the most complete,  
274 encompassing more pits per plot and considering the full soil depth. Prior studies have considered the  
275 SOC stock over a uniform 0-30 cm depth (e.g., Girardin et al., 2014a) or considering separate  
276 horizons to a depth of 50 cm (Zimmermann et al., 2009). Our soil C stock values are a factor of 1.2 to  
277 1.7 higher than values reported in these previous studies (Girardin et al., 2014a; Zimmermann et al.,  
278 2009). For the same soil pit data (i.e., density and %C) used in this study, calculation of soil C stocks  
279 over depths equivalent to those used in the prior studies (i.e., over the top 0-30 cm and 0-50 cm)  
280 yields values in close agreement with those previously reported (see Supplement Fig. S1). This  
281 consistency indicates that the differences between the full-depth values used here, versus the partial  
282 depth values reported previously, are attributable predominantly to the integration depth used.

283 We use the SOC stock data to estimate the amount of soil carbon removed by landslides. These data  
284 may provide an upper estimate on the total amount of organic carbon derived from recently  
285 photosynthesized biomass (i.e., “biospheric organic carbon”), partly because of the presence of  
286 carbonate C and rock-derived organic carbon which is present in the catchment (Clark et al., 2013).  
287 However, the contribution from these non-biospheric components is expected to be small given the  
288 relatively low content of each compared to biospheric %OC, typically at concentrations of many  
289 percent. Additional bias may arise from the location of plots within the catchment, specifically with  
290 respect to topographic position (Marvin et al., 2014). The mean plot slopes range from 20° to 38°, as  
291 measured from the 3 m x 3 m CAO DEM, so these sites capture a large slope range but are at the  
292 lower slope end of the slopes found throughout the Kosñipata catchment (mean catchment slope of  
293 38°). Data on soil OC stocks collected from a wide range in slopes at high elevations (near the tree  
294 line) in the region of the Kosñipata Valley suggest there is not an evident slope-dependence that  
295 would be likely to strongly bias our results (see Supplement Fig. S2; Gibbon et al., 2010).

296

### 297 **3.3.3. Calculating fluxes of carbon stripped from hillslopes by landslides**

298 Carbon stocks for soil, above ground living biomass, and roots were calculated for elevation bands of  
299 300 m, based on the relationships in Table 1. Landslide carbon flux ( $\text{tC yr}^{-1}$ ) was determined by  
300 multiplying the landslide rate in each elevation band ( $\% \text{ yr}^{-1}$ ) by soil, AGLB, and root carbon stocks  
301 ( $\text{tC km}^{-2}$ ) in the respective elevation band. We propagated the error on the elevation trends (from Fig.  
302 7 and Table 1) to estimate uncertainty on the landslide-associated carbon flux by Gaussian error  
303 propagation. The landslide C yield ( $\text{tC km}^{-2} \text{ yr}^{-1}$ ) was calculated by summing all 300 m elevation  
304 bands and normalising by the non-shadow catchment area ( $143 \text{ km}^2$ ).

305 The calculations assume that landslides strip all above ground, root biomass and soil material from  
306 hillslopes. This assumption is supported by field observations from the Kosñipata Valley that  
307 landslides are cleared of visible vegetation and roots and are typically bedrock failures that remove  
308 the entire mobile soil layer. To test this latter assumption, we used geometric scaling relationships for  
309 landslides in mountainous terrain (Larsen et al., 2010) to estimate landslide depths. We calculated  
310 landslide volume from the area (A)-volume (V) relationship,  $V = \alpha A^\gamma$ , where  $\alpha$  and  $\gamma$  are scaling  
311 parameters (we used  $\alpha = 0.146$  and  $\gamma = 1.332$ , from the compilation of global landslides in Larsen et  
312 al., 2010, but also tested other literature values). We estimated average depth by dividing volume for  
313 each landslide by the respective landslide area.

### 314 **3.4. Landslide revegetation**

315 We classified landslides as being “revegetated” when they were dominated by a closed forest canopy  
316 to an extent that we could no longer visually distinguish the landslide scar or bare ground in the 2 m

317 resolution WorldView-2 imagery (Blodgett and Isacks, 2007). We determined the fraction of area of  
318 the landslides occurring in each year (beginning in 1988) that was no longer visible as of 2011, the  
319 year with the latest high-resolution image (Fig. 8). Some landslides were revegetated as soon as four  
320 years after occurrence. For landslide years prior to 2008, i.e. all landslide years with some observable  
321 recovery, we ran a linear regression between landslide area revegetated (specifically, area of fully  
322 revegetated landslides from a given year as a % of total landslide area from that year) and the number  
323 of years that had passed since landslide occurrence (the difference between the given year and 2011).  
324 This analysis used a total of 18 data points, one for each year between 1988 and 2007 except for 2  
325 years that had no measured landslides (Fig. 8; Table S2).

326 The metric of visible revegetation that we use in this study provides a measurable index for assessing  
327 ecosystem recovery from remote imagery. However, it does not necessarily mean complete  
328 replenishment of above ground carbon stocks or regrowth of all vegetation to the extent present prior  
329 to landslide removal. It is also likely to take longer than this time for replenishment of soil carbon  
330 stocks to pre-landslide values (Restrepo et al., 2009).

### 331 **3.5. Topographic analysis**

332 We used two DEMs for topographic analysis. Slope angles and elevation statistics within the  
333 Kosñipata catchment study area were calculated from the 3m x 3m CAO LiDAR-based DEM (see  
334 Appendix A). For river channel analysis within the Kosñipata Valley and for all topographic analyses  
335 in the wider Madre de Dios region, we used a 30 m resolution SRTM-derived DEM (Farr et al., 2007)  
336 with holes patched using the ASTER GDEM (METI/NASA, 2009). We were not able to use the  
337 higher-resolution CAO DEM for these calculations because it did not extend beyond the Kosñipata  
338 catchment study area and contained gaps that made complete flow routing calculations problematic.

339 The dependence of calculated slope on grid resolution (Lin et al., 2008; Blodgett and Isacks, 2007;  
340 Zhang and Montgomery, 1994) means that reported slope values inherently differ between the DEMs  
341 used in this study, and when compared to values from the 90 m x 90 m SRTM-derived DEM (cf.  
342 Clark et al., 2013). In this study, we only compare results internally between values calculated from  
343 the same DEM.

344

## 345 **4. Results**

### 346 **4.1. Landslide rates and role of a large rain storm in 2010**

347 Approximately 2% (2.8 km<sup>2</sup>) of the visible Kosñipata Valley study area experienced landslides over  
348 the 25-year study period. This percentage of landslide area is similar to landslide coverage in the

349 Ecuadorian and Bolivian Andes (Blodgett and Isacks, 2007; Stoyan, 2000). Of the total landslide area  
350 in the catchment, 97.1% was in the forested portion and the remaining 2.9% in the puna.

351 The mean valley-wide landslide rates were  $0.076\% \text{ yr}^{-1}$ , when averaged across  $1 \times 1 \text{ km}$  grid cells.  
352 Rates ranged from no landslides detected to  $0.85\% \text{ yr}^{-1}$  for individual grid cells (Fig. 2b). The average  
353 landslide rate corresponds to average hillslope turnover time of  $\sim 1320$  yrs for the valley (Fig. 2c).  
354 Values reported provide a minimum constraint on landslide rate and a maximum constraint on  
355 turnover time, since small landslides and landslides under topographic shadow were excluded (see  
356 Section 3.1). The landslide hillslope turnover time in the Kosñipata Valley is similar to the landslide  
357 hillslope turnover time observed in the Waitangitaona Basin of New Zealand, but is 2.3 times faster  
358 than the mean landscape-scale landslide hillslope turnover in the western Southern Alps of New  
359 Zealand (Hilton et al., 2011) and in Guatemala (Restrepo and Alvarez, 2006) and 24 times faster than  
360 in Mexico and in Central America (Restrepo and Alvarez, 2006).

361 A single large-magnitude rainfall event on March 4<sup>th</sup> 2010 triggered 27% of all of the landslide area  
362 observed during the 25-year study period in the Kosñipata study catchment. Rainfall during this storm  
363 peaked at  $94 \text{ mm hr}^{-1}$ , with  $\sim 200 \text{ mm}$  falling in 4 hr, recorded by a meteorology station at 1350 m  
364 within the catchment (Fig. 9). The storm accounted for  $\sim 185$  landslides with  $0.75 \text{ km}^2$  cumulative  
365 area. The annual total landslide area for 2010 was consequently much higher than for any other year  
366 in the dataset (Fig. 3).

#### 367 **4.2. Spatial patterns of landslides**

368 The histogram of catchment area in the Kosñipata catchment shows a skewed distribution with respect  
369 to elevation, with greater area at lower elevations (Fig. 5a). The histogram of landslide area is shifted  
370 to lower elevations compared to the catchment and shows a bi-modality. The 2010 landslides focused  
371 almost exclusively at low elevations, below  $\sim 2600 \text{ m}$  (Fig. 5c). Although the remaining landslides  
372 over the 25-year study period located at low elevations relative to the catchment, they were at higher  
373 elevations than the 2010 landslides. The bi-modality of the overall landslide distribution emerges  
374 from the addition of the two nearly distinct distributions (Fig. 5c). Because of the small catchment  
375 area at low elevations, overall landslide susceptibility is highest at the low elevations (particularly  
376  $< \sim 1800 \text{ m}$ ) (Fig. 5b). When excluding the 2010 landslides, the high susceptibility at low elevations is  
377 not evident, and the only clear trend is the very low landslide susceptibility at the highest elevations  
378 ( $> 3500 \text{ m}$ ) (Fig. 5d). Since our mapping did not distinguish landslide scars from deposits (see  
379 Section 3.1), systematic changes in the ratio of scar to deposit area with elevation could influence  
380 | apparent patterns of landslide occurrence and landslide mobilised carbon. For example, larger deposit  
381 | areas at low elevation would increase calculated susceptibility even if the total landslide scar area  
382 | were not larger, though we have no direct evidence to suggest that this is the case. However, our  
383 | anecdotal field observations do not suggest that landslides at lower elevations have consistently longer

384 ~~run-out or larger deposit areas, so it is unlikely that such bias explains the observed relations between~~  
385 ~~landslide occurrence and topography within our inventory.~~

386 The catchment area has a mean slope of 38° (calculated from the CAO DEM) and is skewed to lower  
387 slopes (Figs. 2d, 6a). The distribution of landslide areas is shifted to slightly higher slopes compared  
388 to catchment area and lacks the broad abundance at slopes <30°. The 2010 landslides show a similar  
389 distribution with respect to slope as the landslides from all other years (Fig. 6c). In all cases, landslide  
390 susceptibility increases sharply for slopes >30-40° (Fig. 6d). All of the landslide data include areas at  
391 low slopes, which we interpret as artefacts related to landslide deposits residing in valley bottoms,  
392 since our mapping routines did not distinguish scars from deposits.

### 393 **4.3. Catchment topographic characteristics**

394 The Kosñipata catchment is characterized by a prominent vertical step knickpoint between  
395 approximately 1600 and 1400 m elevation (Fig. 10a). This knickpoint marks an inflection in the  
396 relationship between upstream drainage area and the slope of the river channel, characteristic of the  
397 transition from colluvial to bedrock or alluvial channels in mountainous settings (Whipple, 2004;  
398 Montgomery and Buffington, 1997) although we recognize that processes such as debris-flow incision  
399 may also influence the form of these relations (Stock and Dietrich, 2003). We used flow routing to  
400 separate the catchment into those slopes that drain into the river system upstream of this transition  
401 zone (as defined by the elevation at the top of the vertical step knickpoint) and those slopes that drain  
402 into the river system downstream of the transition (Fig. 10b). Hillslope angles are, on average, steeper  
403 downstream of the transition than upstream, and the distribution of slope angles downstream lacks the  
404 prominent bulge at relatively low slopes that is observed upstream of the transition. The general  
405 features observed in the Kosñipata study catchment, specifically the transition in the slope-area curves  
406 and the related shift in hillslope angles, also generally characterize the other major rivers draining  
407 from the eastern flank of the Andes in the Alto Madre de Dios (Fig. 11).

### 408 **4.4. Catchment-scale carbon stocks and stripping of carbon by landslides**

409 The estimated catchment-scale carbon stock for the Kosñipata Valley is  $\sim 34\,670 \pm 4545$  tC km<sup>-2</sup>, with  
410  $\sim 27\,680 \pm 4420$  tC km<sup>-2</sup> in soil and  $\sim 5370 \pm 840$  tC km<sup>-2</sup> in vegetation (Fig. 7). We estimate that  
411 epiphyte (Horwath, 2011) and woody debris (Gurdak et al., 2014) biomass adds an additional  $\sim 7\%$  of  
412 carbon (<5% from epiphytes and <3% from woody debris; Fig. 7c). Overall, the vegetation carbon  
413 stock values from the Kosñipata Valley are slightly lower than lowland tropical forests, and the soil  
414 values higher (Dixon et al., 1994), which is consistent with broad trends in the tropics in which soil  
415 carbon stocks increase with elevation and are frequently greater than vegetation carbon stocks  
416 (Gibbon et al., 2010; Raich et al., 2006).

417 Averaged over the 25-year duration across the 143 km<sup>2</sup> non-shadowed catchment area, the estimated  
418 total flux of carbon stripped from hillslopes by landslides was 3700±510 tC yr<sup>-1</sup>, with 2880±500 tC yr<sup>-1</sup>  
419 <sup>1</sup> derived from soil and 820±110 tC yr<sup>-1</sup> from vegetation (Fig. 12a). In terms of area-normalized yield  
420 of carbon, landslides stripped 26±4 tC km<sup>-2</sup> yr<sup>-1</sup> from hillslopes, with 20±3 tC km<sup>-2</sup> yr<sup>-1</sup> derived from  
421 soil and 5.7±0.8 tC km<sup>-2</sup> yr<sup>-1</sup> from vegetation (Table 2; Fig. 12b). These values may underestimate  
422 total catchment-wide fluxes because our landslide mapping process missed a proportion of small,  
423 numerous landslides (see Fig. 4, Section 3.1).

424 On the other hand, our values may overestimate fluxes from soil OC if landslides are shallower than  
425 soil depths, since we have assumed complete stripping of soil material to full soil depth and since soil  
426 OC stocks depend on depth of integration (see Section 3.3, above). The deepest average soil depths  
427 observed in the plots used in this study were 1.58 m (Table S3). Using average scaling parameters for  
428 global landslides (Larsen et al., 2010), only 99 landslides in our inventory, equating to 0.06 km<sup>2</sup> total  
429 landslide area (or ~2% of total landslide area), would be shallower than these deepest soils at 1.58 m.  
430 Using scaling parameters for bedrock landslides only ( $\alpha = 0.146$  and  $\gamma = 1.332$ ; Larsen et al. 2010,  
431 results in only one landslide shallower than 1.58 m. This analysis corroborates our field observations  
432 that most landslides in the Kosñipata Valley clear soil from hillslopes and expose bedrock. We thus  
433 view our calculation of fluxes on the basis of complete stripping of soil as providing a reasonable  
434 estimate.

435 Our calculation of landslide-associated carbon fluxes includes carbon that was previously residing  
436 both on landslide scars and in areas of landslide deposits. The fate of carbon from each of these areas  
437 may differ, but such differences are not well known and we consider all to contribute to the loss of  
438 previously living biomass as a result of landslide occurrence. When considering carbon budgets at the  
439 landscape-scale, the landslide-associated carbon fluxes we report here should also be viewed in the  
440 context that other processes such as soil creep may additionally contribute to the transfer of carbon  
441 from hillslopes to rivers (e.g., Yoo et al., 2005).

442

## 443 **5. Discussion**

### 444 **5.1. The geomorphic ‘work’ of storm-triggered landslides in the Kosñipata Valley**

445 The March 2010 storm clearly stands out as the most significant landslide event that occurred during  
446 the duration of this study. We lack a precipitation record for the full 25-year study period, but it is  
447 probable that this storm was the largest single precipitation event during that time. Landslides  
448 triggered in 2010 account for 0.75 km<sup>2</sup>, or 27% of the total landslide area during the 25-year study  
449 period, and these landslides stripped 25,500 tC from hillslopes, equivalent to 26% of the total. The  
450 quantitative importance of this individual storm in our dataset is consistent with observations of

451 storm-triggering of intense landslides elsewhere (Wohl and Ogden, 2013; Ramos Scharrón et al.,  
452 2012; West et al., 2011; Casagli et al., 2006).

453 The annual resolution of our observations of landslide rates in the Kosñipata Valley makes it possible  
454 to consider how the geomorphic work done in this relatively infrequent but high magnitude event  
455 compares to the work done in smaller but more frequent events. Here we define geomorphic work,  
456 *sensu* Wolman and Miller (1960), as total landslide area, reflecting the removal of material from  
457 hillslopes (rather than, for example, the work done by landslides to modify slope angles). Across the  
458 25-year dataset, we estimate the return time or recurrence interval RI (i.e., how frequently a year of  
459 given total landslide magnitude would be expected to occur), as  $RI_i = (n+1)/m_i$ , where  $RI_i$  is the return  
460 interval for the year with the  $i^{\text{th}}$  largest total annual landslide area,  $n$  is the total length of the record  
461 (25 years in this study) and  $m_i$  is the rank order of year  $i$  within the dataset in terms of total landslide  
462 area. Thus 2010, the year with most landslide area, has  $RI = 26$  years, while years characterized by  
463 lower landslide area have more frequent inferred recurrence intervals. When the annual data for  
464 landslide area are plotted as a function of RI (Fig. 3b), 2010 is clearly at the highest magnitude, as a  
465 result of the March 2010 storm. Even so, the landslide area from 2010 still falls on an approximately  
466 linear (power law exponent  $\sim 1$ ) trend coherent with the rest of the dataset. We do not have high  
467 enough temporal resolution to analyse the effects of individual storms in detail, as would be preferred  
468 for a robust recurrence interval analysis. Nonetheless, the linearity of the relationship for annual  
469 landslide areas suggests that even as the frequency of large storm events in the Kosñipata Valley  
470 decreases, the landslide area associated with these events may increase commensurately, such that the  
471 effects compensate.

472 We can further explore the amount of work done, again in terms of landslide area, by the cumulative  
473 effect of repeated events of small magnitude versus occasional events of larger magnitude. This  
474 analysis allows us to consider the relative importance of years with varying landslide area (cf.  
475 Wolman and Miller, 1960). In other words, does a year like 2010, characterized by very high  
476 landslide magnitude, occur often enough that these years dominate the long-term landslide  
477 record? Or do such years occur so rarely that, despite their high magnitude, they have little  
478 effect over the long term? We calculate the % work done for a year with a given recurrence interval  
479 as  $W_i = (A_i/\Sigma A)/RI_i \times 100$ , where  $A_i$  is the landslide area in year  $i$  and  $\Sigma A$  is the total landslide area in  
480 the full dataset. If  $W_i$  is high for a given year relative to other years, then this year is expected  
481 to have a disproportionately large effect on the long-term record, and vice versa. When our  
482 calculated  $W_i$  is plotted versus  $RI_i$ , (Fig. 3c), we find that most years are characterized by very little  
483 landslide activity (low RI and low  $W$ ). The relatively similar values of  $W$  despite large  
484 differences in landslide area (e.g., consider the very high SA in 2010) reflect the  
485 compensation effect of frequency and magnitude. Thus we expect that the long-term total

486 landslide area resulting from years characterized by storm activity of varying magnitude is, on  
487 average, very similar in this setting. In other words, the landslide work done in years with rare, large  
488 storms is more or less similar to the sum of the total integrated work done in those years with smaller  
489 but more frequent storms.

490 Many previous studies of storm-triggered landslides have focused specifically on storm events (e.g.,  
491 Wohl and Ogden, 2013; Ramos Scharrón et al., 2012; West et al., 2011) and lacked such longer-term  
492 context, although several studies on storm triggers of landslides have been concerned with identifying  
493 threshold storm intensities for failure (e.g., Guzzetti et al., 2007; Glade, 1998; Larsen and Simon,  
494 1993). Time series with higher temporal resolution associated with individual storm events of varying  
495 magnitude rather than annual total landslide areas as used in this study would provide a test of the  
496 inferences made here, and analyses similar to that in this study for storm-triggered landslides in other  
497 settings would help shed more light on how storms contribute to erosional processes in mountain  
498 landscapes. Nonetheless, even though the total work done by large magnitude storms may not exceed  
499 that done by smaller events over the long term, the immediacy of large storm effects may be  
500 important from the perspectives of hazards, fluvial impacts, and biogeochemical processes. For  
501 example, large events will supply large amounts of clastic sediment (Wang et al., 2015) and organic  
502 material (West et al., 2011) in a short space of time.

## 503 **5.2. Spatial patterns of landslide activity**

### 504 **5.2.1 Spatial patterns and their relation to the 2010 storm**

505 Spatial and temporal patterns of landslides depend on proximal triggers such as rainfall and seismic  
506 activity (Lin et al., 2008; Meunier et al., 2008; Densmore and Hovius, 2000), as well as on  
507 geomorphic pre-conditions, such as bedrock strength and slope angle, the latter of which is at least in  
508 part regulated by fluvial incision by rivers (Larsen and Montgomery, 2012; Bussmann et al., 2008;  
509 Lin et al., 2008). The observation of highest landslide susceptibility in the Kosñipata Valley at highest  
510 slopes in the catchment reflects the importance of slope angle for landslide failure. The notable shift  
511 from low to high landslide susceptibility above 30-40° (Fig. 6b) is consistent with the hillslope angles  
512 that reflect rock strength expected for the metamorphic and plutonic bedrock (Larsen and  
513 Montgomery, 2012). Generally, the greater overall landslide susceptibility at the lower elevations in  
514 the Kosñipata Valley is consistent with the higher slope angles at these elevations (Figs. 2, 5, 10b).  
515 This set of observations is consistent with predictions of a threshold hillslope model (cf. Gallen et al.,  
516 2015; Roering et al., 2015; Larsen and Montgomery, 2012).

517 In more detail, the distribution of landslides with respect to elevation in the Kosñipata Valley is  
518 complicated by clustering of the 2010 storm-triggered landslides at low elevations. This clustering  
519 may be explained at least in part by the focused intensity of the 2010 storm precipitation at low  
520 elevations; much lower rainfall was recorded on March 4<sup>th</sup> at a meteorology station at 2900 m

521 elevation in the Kosñipata Valley (at the Wayqecha forest plot), compared to the San Pedro  
522 meteorological station at 1450 m elevation (Fig. 9a). Although the single 2010 event may not  
523 contribute more to the development of long-term landslide area than the cumulative effect of smaller  
524 events (see above), the landslides from this one specific event do significantly influence the overall  
525 spatial distribution of landslides visible in present-day imagery. One implication of this observation is  
526 that landslide maps based on all visible landslides at any one point in time, assuming uniform rates of  
527 occurrence, may overlook the role of specific proximal triggering events that lead to spatial clustering.  
528 Such event-clustering may influence inferred relationships between landslides and controlling factors  
529 such as regional precipitation gradients or patterns of uplift, emphasizing that time-sequence of  
530 landslide occurrence may be important to accurately assessing such relationships.

### 531 **5.2.2 Storm triggered landslides at low elevations: Stochastic happenstance or characteristic of** 532 **long-term erosional patterns?**

533 The elevation distribution of landslides in the 2010 storm is clearly distinct from the background  
534 landslide activity during the 25-year study period. This difference raises an important question: are the  
535 2010 landslides representative of a distinct spatial pattern associated with larger storm events? Or are  
536 the spatial locations of these landslides reflective of one stochastic storm event that happened to be  
537 captured in our analysis and is part of a series of events that shift in location throughout the catchment  
538 over time? We cannot distinguish these possibilities conclusively, but we do have some evidence that  
539 allows for preliminary inferences that could be tested with further work. Two lines of evidence  
540 suggest that the focusing of storm-triggered landslides at low elevations in the Kosñipata study  
541 catchment may be characteristic of long-term spatial patterns in which routine landslides occur  
542 throughout the catchment while rarer, intense landslide events selectively affect the lower elevations.

543 The first line of evidence is that the magnitude-frequency statistics for precipitation indicate that low-  
544 frequency events of high-magnitude (i.e., relatively infrequent but large storms) are more  
545 characteristic at low elevation sites compared to high elevations (Fig. 9b). This statistical tendency  
546 toward more storm activity at low elevations would provide a mechanism for regular storm-triggering  
547 of landslides at these elevations.

548 A second set of information comes from the Kosñipata Valley topography and its relation to implied  
549 erosion associated with landslide activity. Although total landslide area in our Kosñipata dataset is  
550 greatest at mid-elevations, these mid-elevation landslides are distributed over a relatively large  
551 catchment area (Fig. 5a). Effective landslide erosion is greatest where landslide susceptibility on a  
552 unit-area basis is highest (Fig. 5b), so our inventory implies focused landslide erosion at lower  
553 elevations (<~1500-2000 m) in the Kosñipata Valley, specifically associated with the 2010 storm  
554 (Figs. 2a, 5). This focused erosion appears to spatially coincide with the observed transition in the  
555 river channel profile at ~1700 m elevation, marked by the vertical step knickpoint (Fig. 10a). In the

556 Kosñipata Valley, this transition occurs near a lithological change from sedimentary to plutonic  
557 bedrock. However, as best known the lithological contact does not exactly coincide spatially with the  
558 knickpoint, and the other principal rivers in the region are also characterised by similar transitions in  
559 channel morphology even though they do not have the same lithological transition, suggesting that  
560 lithology is not the primary control on the observed transition in channel morphology (Fig. 11).

561 Several other processes can generate knickpoints in river profiles (e.g., Whipple, 2001). The  
562 topographic transition in the Kosñipata and in neighbouring catchments appears to approximately  
563 coincide with changes in precipitation regime, and specifically with less cloud cover and greater storm  
564 occurrence below the level of most persistent annual cloud cover in the Andean mid-elevations. (cf.  
565 Espinoza et al., 2015 and Rohrmann et al., 2014 for the southern central Andes). By increasing  
566 erosional efficiency, this climatic transition may at least in part contribute to generating the observed  
567 channel profile. Other effects may also be important, for example the transient upstream propagation  
568 of erosion driven by past changes in uplift, as proposed for the eastern Andes in Bolivia (Whipple and  
569 Gasparini, 2014), or unidentified geologic structures in the Alto Madre de Dios region. These  
570 possibilities are discussed further below.

571 Whatever the underlying cause, hillslope angles downstream of the transitions in channel morphology  
572 are generally steeper than those upstream (Figs. 10b and 11c), consistent with the downstream slopes  
573 being more prone to landslide failure over the long term. The total area of landslides triggered on low-  
574 elevation slopes in 2010 does not exceed the accumulated landslide area in the rest of the catchment  
575 over the longer term (see discussion of magnitude-frequency above, and histograms of landslide area  
576 in Fig. 5a). Nonetheless, these low-elevation landslides are concentrated in a smaller area (Fig. 5b)  
577 and therefore represent higher landslide susceptibility, greater rates of landscape lowering and more  
578 frequent hillslope turnover.

579 Based on the consistency of catchment topography with the landslide distribution that includes 2010  
580 storm-triggered landslides, we speculate that the high rates of landslide erosion at low elevations in  
581 the Kosñipata catchment are characteristic of long-term erosional patterns. This hypothesis could be  
582 tested by complementing the landslide analysis presented in this study with measurements of long-  
583 term denudation rates in small tributary basins of the Kosñipata Valley above and below the apparent  
584 morphologic transition. Although we acknowledge that we currently lack such supporting  
585 independent evidence, in the following sections we include consideration of some of the possible  
586 implications of our hypothesized transition towards higher landslide occurrence at lower elevations in  
587 the Kosñipata Valley.

### 588 **5.3. Landslide-driven erosion and regional topography**

589 In general terms, high-elevation, low-slope surfaces, such as those that characterize the upper portions  
590 of the Kosñipata Valley, are thought to have a number of possible origins, including (i) the uplift and

591 preservation of previously low-lying “relict” surfaces (e.g., Clark et al., 2006), (ii) glacial “buzz-saw”  
592 levelling of surfaces near the glacial equilibrium line altitude (Brozović et al., 1997), (iii) erosion of  
593 rocks with contrasting strength (e.g., Oskin and Burbank, 2005), and (iv) in situ generation through  
594 river system reorganization over time (Yang et al., 2015). There is no evidence for a glacial or  
595 lithological cause for low-relief parts of the Kosñipata Valley and the immediately adjacent portions  
596 of the Andean plateau, suggesting either a relict origin or in situ fluvial formation. Similar high-  
597 elevation, low-relief surfaces south of our study region, along the eastern flank of the Andes in  
598 Bolivia, have been proposed as relict landscapes uplifted in the past ~10-12 Myrs (Whipple and  
599 Gasparini, 2014; Barke and Lamb, 2006; Gubbels et al., 1993). By this interpretation, erosion into the  
600 eastern Andean margins has generated escarpments but not yet erased the original surfaces (Whipple  
601 and Gasparini, 2014).

602 From landslide mapping in the Kosñipata Valley, we infer higher hillslope erosion rates at lower  
603 elevations and particularly downstream of the knickpoint in this catchment. Even when ignoring the  
604 very low-elevation landslides associated with the 2010 storm in our dataset, the occurrence of  
605 landslides throughout the 25-year study period are notably shifted to lower elevations compared to the  
606 Kosñipata catchment area (Fig. 5c). This pattern emphasizes that erosion rates are low at the highest  
607 elevations, where slopes are also lower presumably because incision is less pronounced. If our  
608 observed landslide rates reflect long-term erosion, these observations are consistent with the idea that  
609 the low slopes at high elevations in this region of the Andes are preserved because propagation of  
610 more rapid erosion at low elevations has not yet reached the low-slope parts of the landscape. But,  
611 based on the distribution of landslide erosion alone, we cannot distinguish whether the low slope  
612 regions have their origin as relict landscapes or features resulting from fluvial reorganization.

613 The importance of storm triggering for setting the spatial patterns of landslide activity in the  
614 Kosñipata Valley suggests that greater storm frequency (e.g., Fig. 9b) could be an important  
615 mechanism facilitating higher erosion rates at low elevations in this catchment, consistent with  
616 climate variability being a major erosional driver (DiBiase and Whipple, 2011; Lague et al., 2005).  
617 The indication of a mechanistic link between precipitation patterns and erosion in the Kosñipata  
618 catchment may provide clues about how climatic gradients leave an imprint on the topography of the  
619 eastern Andes (e.g., Strecker et al., 2007), potentially superimposed on tectonically-controlled  
620 patterns of transient erosion into the uplifted mountain range (Gasparini and Whipple, 2014).  
621 Although previous studies have considered the role of gradients in precipitation magnitude across  
622 strike of the eastern Andes (e.g., Gasparini and Whipple, 2014; Lowman and Barros, 2014), we note  
623 that little work has considered the role of storm frequency, which our analysis suggests may be  
624 variable and important in setting erosion patterns in this region.

625 Based on our landslide dataset and the precipitation statistics for the Kosñipata Valley, we speculate  
626 that the greater precipitation magnitude and frequency of large storm events below the cloud  
627 immersion zone in the eastern Andes of the Madre de Dios basin work to facilitate a combination of  
628 hillslope failure, sediment removal, and river channel incision. Channel incision, facilitated by high  
629 storm runoff and the tools provided by landslide erosion (e.g., Crosby et al., 2007), increases hillslope  
630 angles, and landslide failure keeps pace, triggered by storm events such as the 2010 event observed in  
631 our dataset. Focused, climatically controlled erosion at lower elevations along the eastern flank of the  
632 Andes in the Madre de Dios basin could contribute to the preservation of relatively low-slope surfaces  
633 at high elevations: if rates of erosion in and above the cloud immersion zone are limited by decreased  
634 precipitation and particularly reduced storm frequency, the upstream propagation of erosion may be  
635 inhibited, reducing the potential for rivers to incise into the low slope regions in the high-elevation  
636 headwaters. This, in turn, may explain why rivers along the eastern flank of the Andes in Peru have  
637 not succeeded in eroding back into the Andean topography sufficiently to “capture” the flow of the  
638 Altiplano rivers (e.g., the tributaries of the Rio Urubamba that currently flow several hundred  
639 kilometres to the north via the Ucayali before cutting east through the Andes to join the Amazonas).  
640 Our results thus raise the possibility of a potential climatic mechanism for sustaining this topographic  
641 contrast and prolonging the persistence of the asymmetric morphology in this region of the Andes.

#### 642 **5.4. Landslide transfer of organic carbon to rivers**

643 The  $26 \pm 4 \text{ tC km}^{-2} \text{ yr}^{-1}$  of organic carbon stripped from hillslope soil and vegetation during our study  
644 period reflects a significant catchment-scale carbon transfer (Stallard, 1998). The area-normalized  
645 landslide carbon yield in the Kosñipata Valley is similar to the upper end of values for other mountain  
646 sites around the world where analogous carbon fluxes have been evaluated. For example, in a region  
647 of Guatemala with a 20-year hurricane return time, landslide carbon yields were  $33 \text{ tC km}^{-2} \text{ yr}^{-1}$   
648 (Ramos Scharrón et al., 2012), similar to our Kosñipata results. In the western Southern Alps of New  
649 Zealand, landslide carbon yields were  $17 \pm 6 \text{ tC km}^{-2} \text{ yr}^{-1}$  in catchments where landslide rates were  
650 highest, while the mean yield was much lower, at  $\sim 8 \text{ tC km}^{-2} \text{ yr}^{-1}$  (Hilton et al., 2011). In part, the high  
651 carbon flux we observe in the Kosñipata Valley reflects the high organic carbon stocks of soils in this  
652 catchment ( $27\,680 \pm 4\,420 \text{ tC km}^{-2}$ ), larger than the mean estimated in the western Southern Alps,  
653 New Zealand ( $18\,000 \pm 9\,000 \text{ tC km}^{-2}$ ; Hilton et al., 2011). The high flux can also be attributed to the  
654 high rates of landsliding driven by the combination of steep topography and intense precipitation  
655 events (and presumably on multi-centennial timescales by large earthquakes).

656 Following the recolonization of landslide scars (Fig. 8), the fate of landslide-derived organic carbon  
657 governs whether erosion acts as a source or sink of carbon dioxide to the atmosphere (Ramos  
658 Scharrón et al., 2012; Hilton et al., 2011). Bedrock landslides may supply organic carbon to rivers at  
659 the same point in time and space as large amounts of clastic sediment are delivered from hillslopes

660 (Hilton et al., 2011; Hovius et al., 1997). The association of organic matter with high mineral loads  
661 enhances its potential for sedimentary burial and longer-term sequestration of atmospheric carbon  
662 dioxide (Galy et al., 2015; Hilton et al., 2011). In contrast, oxidation of biospheric organic carbon  
663 eroded by landslides represents a poorly quantified source of CO<sub>2</sub> for assessments of ecosystem  
664 carbon balance.

665 The extent to which landslides connect to river channels exerts a first-order control on the fate of  
666 landslide material (Dadson et al., 2004), and thus on the fate of carbon. We identified landslides as  
667 connected or unconnected to rivers by manually inspecting high-resolution imagery and following  
668 landslides to their termination (i.e. to their lowest elevation point). Connected landslides terminated in  
669 river channels, identifiable by the absence of vegetation. We found that, for the Kosñipata Valley  
670 during our study period, greater than 90% of landslides were directly connected with rivers, similar to  
671 the high connectivity found for other storm-triggered landslides (e.g., West et al., 2011). However,  
672 even with high connectivity, it remains uncertain in the case of the Kosñipata how much of the  
673 material stripped by landslides is actually removed by rivers and exported out of the valley.

674 While quantifying the onward fluvial transfer of organic carbon stripped by landslides and its fate in  
675 the Madre de Dios River and wider Amazon Basin is out of the scope of the present study, our  
676 observations provide baseline data for interpreting river flux measurements, as well as important new  
677 insight on the role of landslides in the routing of organic carbon in mountain catchments. First, we  
678 note that the location of landslides within a catchment may influence whether the organic material  
679 eroded from hillslopes is transported by rivers (Hilton et al., 2008b). The observation that landslide  
680 erosion may be non-uniform thus has important implications for organic carbon fate. In lower-order  
681 streams, landslides may be less likely to connect to rivers (Ramos Scharrón et al., 2012), and rivers  
682 are less likely to have capacity to export material, compared to higher order streams. In the Kosñipata  
683 River, focused erosion of organic carbon occurs in the low/mid-elevations and is likely to act to  
684 enhance delivery into higher order river channels, optimizing the potential for removal from the river  
685 catchment. For instance, the mid-elevations (2100 m to 3000 m) are the source of the majority (51%)  
686 of the organic material (in terms of mass per time) eroded from hillslopes by landslides, because these  
687 elevations cover the greatest proportion of total basin area (43%) (Fig. 12a). On a per-area basis (i.e.,  
688 in tC km<sup>-2</sup> yr<sup>-1</sup>), landslide mobilisation of organic carbon is most frequent at lower elevations (Fig.  
689 12b); while the land area in the Kosñipata study area below 1800 m elevation comprises 9% of the  
690 total catchment area, 18% of the organic material stripped by landslides comes from these elevations  
691 (Figs. 12a, 12b).

692 Second, the landslide-derived organic carbon yield is mostly (80%) derived from soil organic matter.  
693 This material is finer-grained than coarse woody debris and is thus more likely to be entrained and  
694 transported by the Kosñipata River. This observation is consistent with measurements of the isotopic

695 and elemental composition of river-borne particulate organic carbon (POC) in this catchment, which  
696 suggest that soil organic carbon from upper horizons appears to be a significant source of biospheric  
697 POC (Clark et al., 2013). While the total POC export fluxes from the Kosñipata River are still to be  
698 quantified, it is likely that the landslide process offers a mechanism by which large quantities of  
699 organic matter, and particularly fine-grained soil organic matter susceptible to fluvial transport, can be  
700 supplied from steep hillslopes to river channels.

701 Finally, our observations are important for understanding the episodic delivery of Andean-derived  
702 organic matter to river systems via the landslide process. The distinct focusing of 2010 rain storm-  
703 driven erosion at low elevations of the Kosñipata study catchment demonstrates the potential for  
704 landslides triggered by individual storm events to erode material selectively from within a  
705 catchment's elevation range. Measurements of biomarker isotope composition in downstream river  
706 sediment have shown that organic erosional products reflect distinct elevation sources during storms  
707 (Ponton et al., 2014). Together, these results emphasize the potential role for storm events to  
708 determine the organic biomarker composition delivered to sediments and to introduce biases relative  
709 to the uniform catchment integration often assumed of erosion (Bouchez et al., 2014; Ponton et al.,  
710 2014).

### 711 **5.5. Timescales of re-vegetation and implications for ecosystem disturbance and composition**

712 The biomass and soil removed by landslides is regenerated on hillslopes over time. The duration and  
713 dynamics of vegetation recovery influence vegetation structure and soil structure, provide habitat for  
714 various species, play an integral role in nutrient cycling, and determine the timescale over which  
715 standing stocks of organic carbon are replenished (Restrepo et al., 2009; Bussmann et al., 2008). For  
716 the Kosñipata study catchment, we estimate that 100% of the landslide area from a given year reaches  
717 full vegetation cover that is indistinguishable from the surrounding vegetation (based on observable  
718 changes from 1988 to 2011 in remote sensing imagery) at  $\sim 27 \pm 8$  yrs after landslide occurrence (Fig.  
719 8). Individual landslides showed large variability; one landslide with a very large area at high  
720 elevation, visible in an air photo from 1963, is still visible with active portions in 2011, indicating that  
721 at least portions of very large landslides may take longer ( $>48$  yrs) to revegetate, partly due to  
722 reactivation. On the other hand, the shortest revegetation time for a landslide occurred within 4 years.  
723 In the Bolivian Andes, at sites with similar montane forest and similar elevation range, similar  
724 revegetation times of 10 to 35 yrs were estimated based on dating trees on landslide scars and  
725 evaluating canopy closure in aerial photographs (Blodgett and Isacks, 2007).

726 Although the return to vegetation cover on landslide scars may occur over several decades, it may  
727 take much longer, perhaps hundreds of years, to reach the full maturity of a tropical montane cloud  
728 forest and to fully replenish soil carbon stocks (Walker et al., 1996). Post-landslide vegetation  
729 modelling in the Ecuadorian Andes (1900-2100 m) suggested that initial return of vegetation to

730 landslide surfaces occurs within 80 years after a landslide but that it takes at least 200 years for the  
731 post-landslide forest to develop the biomass of a mature tropical montane forest (Dislich and Huth,  
732 2012). The timescale of this full maturation process may be important when considering the impact of  
733 landslides on carbon budgets and ecosystem dynamics.

734 Repeated cycles of landslide activity and re-vegetation have the potential to introduce disturbance to  
735 ecosystems that may affect soil nutrient status, carbon stocks, and even plant biodiversity (Restrepo et  
736 al., 2009). Patches of bare rock left by landslides undergo ‘quasi-primary’ succession (Restrepo et al.,  
737 2009) that promotes movement of organisms and ecosystem reorganisation (Walker et al., 2013;  
738 Hupp, 1983), while inhibiting ecosystem retrogression and nutrient depletion (Peltzer et al., 2010). On  
739 landslides in the Bolivian Andes, plant species richness increased from early to late succession and  
740 then declined in very mature or senescent forests (Kessler, 1999).

741 In the Kosñipata Valley, the spatial trends in landslide rate with elevation are similar to trends in plant  
742 species richness measured at forest plots (Fig. 13). Similar to landslide activity, species richness is  
743 lowest at high elevations, increases slightly with decreasing elevation to 2000 m, and then increases  
744 abruptly (from 80 to 180 species ha<sup>-1</sup>) on forested hillslopes between 2000 m and ~1700 m (Fig. 13).  
745 The coincidence of these patterns may reflect the control of both landslides and biodiversity by  
746 climatic conditions (e.g., both greater landslide activity and greater biodiversity below the cloud  
747 immersion zone). Or the patterns may be simply coincidental, with biodiversity regulated by factors  
748 independent of landslide erosion, such as light and temperature, or the transition between  
749 lowland/submontane species and montane cloud forest species. We suggest that it may also be  
750 possible that the intermediate disturbance regime (Connell, 1978) associated with landslide activity at  
751 the lower catchment elevations influences ecosystem structure (Walker et al., 2013; Restrepo et al.,  
752 2009; Kessler, 1999; Hupp, 1983) and contributes to enhanced biodiversity observed below ~1700 m.  
753 Such effects could be consistent with peaks in species richness at mid-elevations (around 1500 m)  
754 observed across Andean forest plots in Peru (Fig. 13), Bolivia, and Ecuador (Engemann et al., 2015;  
755 Salazar et al., 2015; Girardin et al., 2014b; Huaraca Huasco et al., 2014). A complex mix of  
756 geomorphic, climatic and ecological factors likely influence landslide and biodiversity patterns, but  
757 coincidence in our dataset provides impetus for future studies of species diversity along  
758 geomorphically-imposed gradients of disturbance.

759

## 760 **7. Conclusions**

761 We have quantified the spatial and temporal patterns of landslides over 25-years in the Kosñipata  
762 Valley, a forested mountain catchment in the Peruvian Andes. Over the 25 year period, one extreme  
763 rainfall event in 2010 triggered ~1/4 of all inventoried landslides, demonstrating the importance of  
764 large rainfall events for landslide activity in the Andes. The annual data from this study suggest that

765 the cumulative landslide area associated with smaller, more frequent storms may be similar to the area  
766 associated with larger, rarer storms.

767 The landslides mobilized significant amounts of carbon from forested hillslopes, with an average  
768 yield of  $26 \pm 4 \text{ tC km}^{-2} \text{ yr}^{-1}$ . This is one of the largest erosive fluxes of biospheric carbon recorded in a  
769 mountain catchment. We estimate that a large proportion of this material was from soil organic matter  
770 ( $20 \pm 3 \text{ tC km}^{-2} \text{ yr}^{-1}$ ) scoured from depths of  $\sim 1.5\text{m}$  or less, with above- and below-ground biomass  
771 marking a smaller, yet still important contribution ( $5.7 \pm 0.8 \text{ tC km}^{-2} \text{ yr}^{-1}$ ). That coupled with the  
772 observation that  $\sim 90\%$  of the mapped landslide areas were spatially connected to river channels  
773 suggests that this biospheric carbon may be very mobile, and may contribute importantly to suspended  
774 sediment export by the Kosñipata River. The onward fate of this carbon will play an important role in  
775 determining whether landsliding and physical erosion processes in the Andes contributes a net carbon  
776 dioxide source or sink.

777 Landslides observed in this study were not distributed uniformly across the catchment area, but were  
778 focused on slopes above a threshold angle (ca.  $30\text{-}40^\circ$ ), consistent with previous studies and  
779 theoretical expectations. The highest elevations in the catchment are characterized by low slopes and  
780 relatively little landslide activity. Landslides triggered by the large storm in 2010 cluster at low  
781 elevations, where precipitation magnitude-frequency relations and catchment morphology hint that  
782 such pulses of intense erosional activity may be characteristic of long-term patterns. Such non-  
783 uniform erosion would have implications for sources and composition of sediment, organic matter and  
784 associated biomarkers and could potentially contribute to influencing forest species composition  
785 through patterns of disturbance. Relations between storm activity, landsliding and landscape processes  
786 and ecological function merit further investigation to probe these possible links.

787

788 **Appendix A. High-resolution Digital Elevation Model**

789 For analysing the topography of the Kosñipata study catchment, we used a DEM generated from the  
790 Carnegie Airborne Observatory 2 (CAO-2) next generation Airborne Taxonomic Mapping System  
791 (AToMS) with an Airborne Light Detection and Ranging (LiDAR) (Asner et al., 2012). The CAO  
792 data was processed to 1.12 m spot spacing. Laser ranges from the LiDAR were combined with the  
793 embedded high resolution Global Positioning System-Inertial Measurement Unit (GPS-IMU) data to  
794 determine the 3-D locations of laser returns, producing a ‘cloud’ of LiDAR data. The LiDAR data  
795 cloud consists of a very large number of georeferenced point elevation estimates (cm), where  
796 elevation is relative to a reference ellipsoid (WGS 1984). To estimate canopy height above ground,  
797 LiDAR data points were processed to identify which laser pulses penetrated the canopy volume and  
798 reached the ground surface. We used these points to interpolate a raster digital terrain model (DTM)  
799 for the ground surface. This was achieved using a 10 m x 10 m kernel passed over each flight block;  
800 the lowest elevation estimate in each kernel was assumed to be ground. Subsequent points were  
801 evaluated by fitting a horizontal plane to each of the ground seed points. If the closest unclassified  
802 point was  $< 5.5^\circ$  and  $< 1.5$  m higher in elevation, it was classified as ground. This process was  
803 repeated until all points within the block were evaluated. The cell resolution was derived from the  
804 DEM resampled in ArcGIS to a 3 m x 3 m DEM to smooth the topography from a 1.12 m x 1.12 m  
805 DEM. Cells in the topographic shadow area and the area of the catchment with a gap in the data ( $\sim 3$   
806 km<sup>2</sup> centralised in the upper elevations) were removed from this analysis.

807

808 *Author contributions.* K. E. Clark, A. J. West, R. G. Hilton, Y. Malhi, M. New, M. R. Silman, and S.  
809 S. Saatchi designed the study; G. P. Asner and R. E. Martin carried out Carnegie Airborne  
810 Observatory (CAO) data acquisition and analysis; C. A. Quesada carried out the soil stock fieldwork  
811 and geochemical analysis; W. Farfan-Rios and M. R. Silman carried out the above ground living  
812 biomass and plant species diversity fieldwork; A. B. Horwath carried out the bryophyte carbon stock  
813 fieldwork; K. Halladay carried out the MODIS cloud cover analysis; K. E. Clark carried the analysis  
814 under the advisement of A. J. West and with contributions from Y. Malhi and R. G. Hilton. K. E.  
815 Clark and A. J. West prepared the manuscript with contributions from all of the co-authors.

816

817

### 818 **Acknowledgements**

819 This paper is a product of the Andes Biodiversity and Ecosystems Research Group (ABERG). KEC  
820 was funded by the Natural Sciences and Engineering Research Council of Canada (NSERC) and  
821 Clarendon Fund PhD scholarships. AJW was supported to work in the Kosñipata Valley by NSF-EAR  
822 1227192 and RGH was supported by a NERC New Investigator Grant (NE/I001719/1). YM is  
823 supported by the Jackson Foundation and a European Research Council Advanced Investigator Grant  
824 GEM-TRAIT. The Carnegie Airborne Observatory is made possible by the Avatar Alliance  
825 Foundation, Grantham Foundation for the Protection of the Environment, John D. and Catherine T.  
826 MacArthur Foundation, Gordon and Betty Moore Foundation, W. M. Keck Foundation, Margaret A.  
827 Cargill Foundation, Mary Anne Nyburg Baker and G. Leonard Baker Jr., and William R. Hearst III.  
828 We thank D. Knapp, T. Kennedy-Bowdoin, C. Anderson, and R. Tupayachi for CAO data collection  
829 and analysis; M. Palace for the QuickBird-2 satellite images from 2009 and 2010; S. Abele for GIS  
830 advice; S. Moon and G. Hilley for providing Matlab code for slope-area analysis; and S. Feakins and  
831 reviewers of a prior submission for comments. We thank Ken Ferrier and an anonymous referee for  
832 their helpful and insightful reviews.

833

834

835 **References**

- 836 ACCA: Weather data San Pedro station, Asociación para la conservación de la cuenca Amazónica,  
 837 (accessed 01/04/2012), 2012.
- 838 Asner, G. P., Powell, G. V., Mascaro, J., Knapp, D. E., Clark, J. K., Jacobson, J., Kennedy-Bowdoin, T.,  
 839 Balaji, A., Paez-Acosta, G., and Victoria, E.: High-resolution forest carbon stocks and  
 840 emissions in the Amazon, *P Natl. Acad. Sci. USA*, 107, 16738-16742,  
 841 10.1073/pnas.1004875107, 2010.
- 842 Asner, G. P., Knapp, D. E., Boardman, J., Green, R. O., Kennedy-Bowdoin, T., Eastwood, M., Martin, R.  
 843 E., Anderson, C., and Field, C. B.: Carnegie Airborne Observatory-2: Increasing science data  
 844 dimensionality via high-fidelity multi-sensor fusion, *Remote Sens. Environ.*, 124, 454-465,  
 845 10.1016/j.rse.2012.06.012, 2012.
- 846 Asner, G. P., Knapp, D. E., Martin, R. E., Tupayachi, R., Anderson, C. B., Mascaro, J., Sinca, F.,  
 847 Chadwick, K. D., Higgins, M., Farfan, W., Llactayo, W., and Silman, M. R.: Targeted carbon  
 848 conservation at national scales with high-resolution monitoring, *P. Natl. Acad. Sci. USA*, 111,  
 849 E5016-E5022, 10.1073/pnas.1419550111, 2014.
- 850 Barke, R., and Lamb, S.: Late Cenozoic uplift of the Eastern Cordillera, Bolivian Andes, *Earth Planet*  
 851 *Sc. Lett.*, 249, 350-367, 10.1016/j.epsl.2006.07.012, 2006.
- 852 Bilderback, E. L., Pettinga, J. R., Litchfield, N. J., Quigley, M., Marden, M., Roering, J. J., and Palmer, A.  
 853 S.: Hillslope response to climate-modulated river incision in the Waipaoa catchment, East  
 854 Coast North Island, New Zealand, *Geol. Soc. Am. Bull.*, 127, 131-148, 10.1130/B31015.1,  
 855 2015.
- 856 Blodgett, T. A., and Isacks, B. L.: Landslide erosion rate in the eastern cordillera of northern Bolivia,  
 857 *Earth Interact.*, 11, 1-30, 10.1175/2007EI222.1, 2007.
- 858 Bookhagen, B.: High resolution spatiotemporal distribution of rainfall seasonality and extreme  
 859 events based on a 12-year TRMM time series  
 860 <http://www.geog.ucsb.edu/~bodo/TRMM/index.php>, (accessed 06/06/2013), 2013.
- 861 Bouchez, J., Galy, V., Hilton, R. G., Gaillardet, J., Moreira-Turcq, P., Pérez, M. A., France-Lanord, C.,  
 862 and Maurice, L.: Source, transport and fluxes of Amazon River particulate organic carbon:  
 863 insights from river sediment depth-profiles, *Geochim. Cosmochim. Ac.*, 133, 280-298,  
 864 10.1016/j.gca.2014.02.032, 2014.
- 865 Brozović, N., Burbank, D. W., and Meigs, A. J.: Climatic limits on landscape development in the  
 866 Northwestern Himalaya, *Science*, 276, 571-574, 10.1126/science.276.5312.571, 1997.
- 867 Burbank, D. W., Leland, J., Fielding, E., Anderson, R. S., Brozovic, N., Reid, M. R., and Duncan, C.:  
 868 Bedrock incision, rock uplift and threshold hillslopes in the northwestern Himalayas, *Nature*,  
 869 379, 505-510, 10.1038/379505a0, 1996.
- 870 Bussmann, R. W., Wilcke, W., and Richter, M.: Landslides as important disturbance regimes - Causes  
 871 and regeneration, in: *Gradients in a tropical mountain ecosystem of Ecuador*, edited by:  
 872 Beck, E., Bendix, J., Kottke, I., Makeschin, F., and Mosandl, R., *Ecological Studies*, 198,  
 873 Springer-Verlag, Berlin Heidelberg, Germany, 321-330, 2008.
- 874 Cabrera, J., Sébrier, M., and Mercier, J. L.: Plio-Quaternary geodynamic evolution of a segment of the  
 875 Peruvian Andean Cordillera located above the change in the subduction geometry: The  
 876 Cuzco region, *Tectonophysics*, 190, 331-362, 10.1016/0040-1951(91)90437-W, 1991.
- 877 Carlotto Caillaux, V. S., Rodriguez, G., Fernando, W., Roque, C., Dionicio, J., and Chávez, R.: *Geología*  
 878 *de los cuadrángulos de Urubamba y Calca*, Instituto Geológica Nacional, Lima, Peru, 1996.
- 879 Casagli, N., Dapporto, S., Ibsen, M. L., Tofani, V., and Vannocci, P.: Analysis of the landslide triggering  
 880 mechanism during the storm of 20th–21st November 2000, in *Northern Tuscany, Landslides*,  
 881 3, 13-21, 10.1007/s10346-005-0007-y, 2006.
- 882 Clark, K. E., Hilton, R. G., West, A. J., Malhi, Y., Gröcke, D. R., Bryant, C. L., Ascough, P. L., Robles  
 883 Caceres, A., and New, M.: New views on “old” carbon in the Amazon River: Insight from the

884 source of organic carbon eroded from the Peruvian Andes, *Geochem. Geophys. Geosy.*, 14,  
885 1644-1659, 10.1002/ggge.20122, 2013.

886 Clark, K. E., Torres, M. A., West, A. J., Hilton, R. G., New, M., Horwath, A. B., Fisher, J. B., Rapp, J. M.,  
887 Robles Caceres, A., and Malhi, Y.: The hydrological regime of a forested tropical Andean  
888 catchment, *Hydrol. Earth Syst. Sci.*, 18, 5377-5397, 10.5194/hess-18-5377-2014, 2014.

889 Clark, M. K., Royden, L. H., Whipple, K. X., Burchfiel, B. C., Zhang, X., and Tang, W.: Use of a regional,  
890 relict landscape to measure vertical deformation of the eastern Tibetan Plateau, *J. Geophys.*  
891 *Res.-Earth*, 111, 1-23, 10.1029/2005JF000294, 2006.

892 Connell, J. H.: Diversity in tropical rain forests and coral reefs, *Science*, 199, 1302-1310,  
893 10.1126/science.199.4335.1302, 1978.

894 Consbio: Ecosistemas Terrestres de Peru (Data Basin Dataset) for ArcGIS, Covallis, Oregon, USA,  
895 2011.

896 Crosby, B. T., Whipple, K. X., Gasparini, N. M., and Wobus, C. W.: Formation of fluvial hanging  
897 valleys: Theory and simulation, *J. Geophys. Res.-Earth*, 112, 1-20, 10.1029/2006JF000566,  
898 2007.

899 Dadson, S. J., Hovius, N., Chen, H., Dade, W. B., Lin, J.-C., Hsu, M.-L., Lin, C.-W., Horng, M.-J., Chen, T.-  
900 C., Milliman, J., and Stark, C. P.: Earthquake-triggered increase in sediment delivery from an  
901 active mountain belt, *Geology*, 32, 733-736, 10.1130/G20639.1 2004.

902 Densmore, A. L., and Hovius, N.: Topographic fingerprints of bedrock landslides, *Geology*, 28, 371-  
903 374, 10.1130/0091-7613(2000)28<371:TFOBL>2.0.CO;2 2000.

904 DiBiase, R. A., and Whipple, K. X.: The influence of erosion thresholds and runoff variability on the  
905 relationships among topography, climate, and erosion rate, *J. Geophys. Res.-Earth*, 116, 1-  
906 17, 10.1029/2011JF002095, 2011.

907 Dislich, C., and Huth, A.: Modelling the impact of shallow landslides on forest structure in tropical  
908 montane forests, *Ecol. Model.*, 239, 40-53, 10.1016/j.ecolmodel.2012.04.016, 2012.

909 Dixon, R. K., Brown, S., Houghton, R., Solomon, A., Trexler, M., and Wisniewski, J.: Carbon pools and  
910 flux of global forest ecosystems, *Science*, 263, 185-189, 1994.

911 Egholm, D. L., Knudsen, M. F., and Sandiford, M.: Lifespan of mountain ranges scaled by feedbacks  
912 between landsliding and erosion by rivers, *Nature*, 498, 475-478, 10.1038/nature12218,  
913 2013.

914 Ekström, G., and Stark, C. P.: Simple scaling of catastrophic landslide dynamics, *Science*, 339, 1416-  
915 1419, 10.1126/science.1232887, 2013.

916 Engemann, K., Enquist, B. J., Sandel, B., Boyle, B., Jørgensen, P. M., Morueta-Holme, N., Peet, R. K.,  
917 Violle, C., and Svenning, J.-C.: Limited sampling hampers "big data" estimation of species  
918 richness in a tropical biodiversity hotspot, *Ecol. Evol.*, 5, 807-820, 10.1002/ece3.1405, 2015.

919 Espinoza, J. C., Chavez, S., Ronchail, J., Junquas, C., Takahashi, K., and Lavado, W.: Rainfall hotspots  
920 over the southern tropical Andes: Spatial distribution, rainfall intensity, and relations with  
921 large-scale atmospheric circulation, *Water Resour. Res.*, 51, 1-17, 10.1002/2014WR016273,  
922 2015.

923 Eswaran, H., Van Den Berg, E., and Reich, P.: Organic Carbon in Soils of the World, *Soil Sci. Soc. Am.*  
924 *J.*, 57, 192-194, 10.2136/sssaj1993.03615995005700010034x, 1993.

925 Farr, T. G., Rosen, P. A., Caro, E., Crippen, R., Duren, R., Hensley, S., Kobrick, M., Paller, M.,  
926 Rodriguez, E., Roth, L., Seal, D., Shaffer, S., Shimada, J., Umland, J., Werner, M., Oskin, M.,  
927 Burbank, D., and Alsdorf, D.: The Shuttle Radar Topography Mission, *Rev. Geophys.*, 45,  
928 RG2004, 10.1029/2005RG000183, 2007.

929 Ferrier, K. L., Huppert, K. L., and Perron, J. T.: Climatic control of bedrock river incision, *Nature*, 496,  
930 206-209, 10.1038/nature11982, 2013.

931 Gallen, S. F., Clark, M. K., and Godt, J. W.: Coseismic landslides reveal near-surface rock strength in a  
932 high-relief tectonically active setting, *Geology*, 43, 70-70, 10.1130/G36080.1 2015.

933 Galy, V., Peucker-Ehrenbrink, B., and Eglinton, T.: Global carbon export from the terrestrial  
934 biosphere controlled by erosion, *Nature*, 521, 204-207, 10.1038/nature14400, 2015.

935 Gasparini, N. M., and Whipple, K. X.: Diagnosing climatic and tectonic controls on topography:  
936 Eastern flank of the northern Bolivian Andes, *Lithosphere*, 6, 230-250, 10.1130/l322.1, 2014.

937 Gibbon, A., Silman, M. R., Malhi, Y., Fisher, J. B., Meir, P., Zimmermann, M., Dargie, G. C., Farfan, W.  
938 R., and Garcia, K. C.: Ecosystem carbon storage across the grassland-forest transition in the  
939 high Andes of Manu National Park, Peru, *Ecosystems*, 13, 1097-1111, 10.1007/s10021-010-  
940 9376-8, 2010.

941 Gilbert, G. K.: *Geology of the Henry Mountains*, *Geology of the Henry Mountains*, Washington, D.C.,  
942 Report, i-160 pp., 1877.

943 Girardin, C. A. J., Malhi, Y., Aragao, L. E. O. C., Mamani, M., Huasco, W. H., Durand, L., Feeley, K. J.,  
944 Rapp, J., Silva-Espejo, J. E., Silman, M., Salinas, N., and Whittaker, R. J.: Net primary  
945 productivity allocation and cycling of carbon along a tropical forest elevational transect in  
946 the Peruvian Andes, *Glob. Change Biol.*, 16, 3176-3192, 10.1111/j.1365-2486.2010.02235.x,  
947 2010.

948 Girardin, C. A. J., Aragão, L. E. O. C., Malhi, Y., Huaraca Huasco, W., Metcalfe, D. B., Durand, L.,  
949 Mamani, M., Silva-Espejo, J. E., and Whittaker, R. J.: Fine root dynamics along an elevational  
950 gradient in tropical Amazonian and Andean forests, *Global Biogeochem. Cy.*, 27, 252-264,  
951 10.1029/2011GB004082, 2013.

952 Girardin, C. A. J., Malhi, Y., Feeley, K. J., Rapp, J. M., Silman, M. R., Meir, P., Huaraca Huasco, W.,  
953 Salinas, N., Mamani, M., Silva-Espejo, J. E., García Cabrera, K., Farfan Rios, W., Metcalfe, D.  
954 B., Doughty, C. E., and Aragão, L. E. O. C.: Seasonality of above-ground net primary  
955 productivity along an Andean altitudinal transect in Peru, *J. Trop. Ecol.*, 30, 503-519,  
956 10.1017/S0266467414000443, 2014a.

957 Girardin, C. A. J., Silva-Espejo, J. E., Doughty, C. E., Huaraca Huasco, W., Metcalfe, D. B., Durand-Baca,  
958 L., Marthews, T. R., Aragao, L. E. O. C., Farfan Rios, W., García Cabrera, K., Halladay, K.,  
959 Fisher, J. B., Galiano-Cabrera, D. F., Huaraca-Quispe, L. P., Alzamora-Taype, I., Equiluz-Mora,  
960 L., Salinas-Revilla, N., Silman, M., Meir, P., and Malhi, Y.: Productivity and carbon allocation  
961 in a tropical montane cloud forest of the Peruvian Andes, *Plant Ecol. Divers.*, 7, 107-123,  
962 10.1080/17550874.2013.820222, 2014b.

963 Glade, T.: Establishing the frequency and magnitude of landslide-triggering rainstorm events in New  
964 Zealand, *Eng. Geol.*, 35, 160-174, 10.1007/s002540050302, 1998.

965 Gregory-Wodzicki, K. M.: Uplift history of the Central and Northern Andes: A review, *Geol. Soc. Am.*  
966 *Bull.*, 112, 1091-1105, 10.1130/0016-7606(2000)112<1091:UHOTCA>2.0.CO;2 2000.

967 Gubbels, T. L., Isacks, B. L., and Farrar, E.: High-level surfaces, plateau uplift, and foreland  
968 development, Bolivian central Andes, *Geology*, 21, 695-698, 10.1130/0091-  
969 7613(1993)021<0695:hlsqua>2.3.co;2, 1993.

970 Gurdak, D. J., Aragao, L. E. O. C., Rozas-Dávila, A., Huaraca Huasco, W., García Cabrera, K., Doughty,  
971 C. E., Farfan-Rios, W., Silva-Espejo, J. E., Metcalfe, D. B., Silman, M. R., and Malhi, Y.:  
972 Assessing above-ground woody debris dynamics along a gradient of elevation in Amazonian  
973 cloud forests in Peru: balancing above-ground inputs and respiration outputs, *Plant Ecol.*  
974 *Divers.*, 7, 143-160, 10.1080/17550874.2013.818073, 2014.

975 Guzzetti, F., Peruccacci, S., Rossi, M., and Stark, C. P.: Rainfall thresholds for the initiation of  
976 landslides in central and southern Europe, *Meteorol. Atmos. Phys.*, 98, 239-267,  
977 10.1007/s00703-007-0262-7, 2007.

978 Halladay, K., Malhi, Y., and New, M.: Cloud frequency climatology at the Andes/Amazon transition: 1.  
979 Seasonal and diurnal cycles, *J. Geophys. Res.*, 117, D23102, 10.1029/2012JD017770, 2012.

980 Hilton, R. G., Galy, A., and Hovius, N.: Riverine particulate organic carbon from an active mountain  
981 belt: Importance of landslides, *Global Biogeochem. Cy.*, 22, BG1017,  
982 10.1029/2006GB002905, 2008a.

983 Hilton, R. G., Galy, A., Hovius, N., Chen, M.-C., Horng, M.-J., and Chen, H.: Tropical-cyclone-driven  
984 erosion of the terrestrial biosphere from mountains, *Nat Geosci*, 1, 759-762,  
985 10.1038/ngeo333, 2008b.

986 Hilton, R. G., Meunier, P., Hovius, N., Bellingham, P. J., and Galy, A.: Landslide impact on organic  
987 carbon cycling in a temperate montane forest, *Earth Surf. Proc. Land.*, 36, 1670-1679,  
988 10.1002/esp.2191, 2011.

989 Hilton, R. G., Gaillardet, J., Calmels, D., and Birck, J.-L.: Geological respiration of a mountain belt  
990 revealed by the trace element rhenium, *Earth Planet Sc. Lett.*, 403, 27-36,  
991 10.1016/j.epsl.2014.06.021, 2014.

992 Horwath, A.: Epiphytic bryophytes as cloud forest indicators: Stable isotopes, biomass and diversity  
993 along an altitudinal gradient in Peru, Doctor of Philosophy, Plant Sciences, University of  
994 Cambridge, Cambridge, 260 pp., 2011.

995 Hovius, N., Stark, C. P., and Allen, P. A.: Sediment flux from a mountain belt derived by landslide  
996 mapping, *Geology*, 25, 231-234, 10.1130/0091-7613(1997)025<0231:sffamb>2.3.co;2, 1997.

997 Hovius, N., Stark, C. P., Chu, H. T., and Lin, J. C.: Supply and removal of sediment in a landslide-  
998 dominated mountain belt: Central Range, Taiwan, *J. Geol.*, 108, 73-89, 10.1086/314387,  
999 2000.

1000 Huaraca Huasco, W., Girardin, C. A. J., Doughty, C. E., Metcalfe, D. B., Baca, L. D., Silva-Espejo, J. E.,  
1001 Cabrera, D. G., Aragão, L. E. O., Davila, A. R., Marthews, T. R., Huaraca-Quispe, L. P.,  
1002 Alzamora-Taype, I., Eguiluz-Mora, L., Farfan-Rios, W., Cabrera, K. G., Halladay, K., Salinas-  
1003 Revilla, N., Silman, M., Meir, P., and Malhi, Y.: Seasonal production, allocation and cycling of  
1004 carbon in two mid-elevation tropical montane forest plots in the Peruvian Andes, *Plant Ecol.*  
1005 *Divers.*, 1-2, 125-142, 10.1080/17550874.2013.819042, 2014.

1006 Hupp, C. R.: Seedling establishment on a landslide site, *Castanea*, 48, 89-98, 1983.

1007 INGEMMET: GEOCATMIN - Geologia integrada por proyectos regionales, Lima, Peru, 2013.

1008 Keefer, D. K.: The importance of earthquake-induced landslides to long-term slope erosion and  
1009 slope-failure hazards in seismically active regions, *Geomorphology*, 10, 265-284,  
1010 10.1016/0169-555X(94)90021-3, 1994.

1011 Kessler, M.: Plant species richness and endemism during natural landslide succession in a perhumid  
1012 montane forest in the Bolivian Andes, *Ecotropica*, 5, 123-136, 1999.

1013 Lague, D., Hovius, N., and Davy, P.: Discharge, discharge variability, and the bedrock channel profile,  
1014 *J. Geophys. Res.-Earth*, 110, 1-17, 10.1029/2004JF000259, 2005.

1015 Larsen, I. J., Montgomery, D. R., and Korup, O.: Landslide erosion controlled by hillslope material,  
1016 *Nat. Geosci.*, 3, 247-251, 10.1038/ngeo776, 2010.

1017 Larsen, I. J., and Montgomery, D. R.: Landslide erosion coupled to tectonics and river incision, *Nat.*  
1018 *Geosci.*, 5, 468-473, 10.1038/ngeo1479, 2012.

1019 Larsen, M. C., and Simon, A.: A rainfall intensity-duration threshold for landslides in a humid-tropical  
1020 environment, Puerto Rico, *Geogr. Ann. A.*, 75, 13-23, 10.2307/521049, 1993.

1021 Li, G., West, A. J., Densmore, A. L., Jin, Z., Parker, R. N., and Hilton, R. G.: Seismic mountain building:  
1022 Landslides associated with the 2008 Wenchuan earthquake in the context of a generalized  
1023 model for earthquake volume balance, *Geochem. Geophys. Geosy.*, 15, 833-844,  
1024 10.1002/2013GC005067, 2014.

1025 Lin, G.-W., Chen, H., Hovius, N., Horng, M.-J., Dadson, S., Meunier, P., and Lines, M.: Effects of  
1026 earthquake and cyclone sequencing on landsliding and fluvial sediment transfer in a  
1027 mountain catchment, *Earth Surf. Proc. Land.*, 33, 1354-1373, 10.1002/esp.1716, 2008.

1028 Lowman, L. E. L., and Barros, A. P.: Investigating links between climate and orography in the Central  
1029 Andes: Coupling erosion and precipitation using a physical-statistical model, *J. Geophys.*  
1030 *Res.-Earth*, 119, 1322-1353, 10.1002/2013JF002940, 2014.

1031 Malamud, B. D., Turcotte, D. L., Guzzetti, F., and Reichenbach, P.: Landslide inventories and their  
1032 statistical properties, *Earth Surf. Proc. Land.*, 29, 687-711, 10.1002/esp.1064, 2004.

1033 Malhi, Y., Silman, M., Salinas, N., Bush, M., Meir, P., and Saatchi, S.: Introduction: Elevation gradients  
1034 in the tropics: Laboratories for ecosystem ecology and global change research, *Glob. Change*  
1035 *Biol.*, 16, 3171-3175, 10.1111/j.1365-2486.2010.02323.x, 2010.

1036 Marc, O., and Hovius, N.: Amalgamation in landslide maps: effects and automatic detection, *Nat.*  
1037 *Hazards Earth Syst. Sci.*, 15, 723-733, 10.5194/nhess-15-723-2015, 2015.

1038 Marengo, J. A., Soares, W. R., Saulo, C., and Nicolini, M.: Climatology of the low-level jet east of the  
1039 Andes as derived from the NCEP-NCAR reanalyses: Characteristics and temporal variability, *J.*  
1040 *Climate*, 17, 2261-2280, 10.1175/1520-0442(2004)017<2261:COTLJE>2.0.CO;2, 2004.

1041 Marvin, D. C., Asner, G. P., Knapp, D. E., Anderson, C. B., Martin, R. E., Sinca, F., and Tupayachi, R.:  
1042 Amazonian landscapes and the bias in field studies of forest structure and biomass, *P. Natl.*  
1043 *Acad. Sci. USA*, 111, E5224-E5232, 10.1073/pnas.1412999111, 2014.

1044 Mendivil Echevarría, S., and Dávila Manrique, D.: *Geología de los cuadrángulos de Cuzco y Livitaca*,  
1045 Instituto Geológica Nacional, Lima, Peru, 1994.

1046 METI/NASA: ASTER Global DEM product, NASA EOSDIS Land Processes DAAC USGS Earth Resources  
1047 Observation and Science (EROS) Center Sioux Falls, South Dakota, USA, 2009.

1048 Meunier, P., Hovius, N., and Haines, J. A.: Topographic site effects and the location of earthquake  
1049 induced landslides, *Earth Planet Sc. Lett.*, 275, 221-232, 10.1016/j.epsl.2008.07.020, 2008.

1050 Montgomery, D. R., and Buffington, J. M.: Channel-reach morphology in mountain drainage basins,  
1051 *Geol. Soc. Am. Bull.*, 109, 596-611, 10.1130/0016-7606(1997)109<0596:CRMIMD>2.3.CO;2,  
1052 1997.

1053 Montgomery, D. R.: Slope distributions, threshold hillslopes, and steady-state topography, *Am. J.*  
1054 *Sci.*, 301, 432-454, 10.2475/ajs.301.4-5.432, 2001.

1055 Montgomery, D. R., and Brandon, M. T.: Topographic controls on erosion rates in tectonically active  
1056 mountain ranges, *Earth Planet Sc. Lett.*, 201, 481-489, 10.1016/S0012-821X(02)00725-2,  
1057 2002.

1058 Moon, S., Chamberlain, C. P., Blisniuk, K., Levine, D. H., Rood, D. H., and Hilley, G. E.: Climatic control  
1059 of denudation in the deglaciated landscape of the Washington Cascades, *Nat. Geosci.*, 4,  
1060 469-473, 10.1038/ngeo1159, 2011.

1061 Oskin, M., and Burbank, D. W.: Alpine landscape evolution dominated by cirque retreat, *Geology*, 33,  
1062 933-936, 10.1130/G21957.1, 2005.

1063 Peltzer, D. A., Wardle, D. A., Allison, V. J., Baisden, W. T., Bardgett, R. D., Chadwick, O. A., Condon, L.  
1064 M., Parfitt, R. L., Porder, S., and Richardson, S. J.: Understanding ecosystem retrogression,  
1065 *Ecol. Mongr.*, 80, 509-529, 10.1890/09-1552.1, 2010.

1066 Pepin, E., Guyot, J. L., Armijos, E., Bazan, H., Fraizy, P., Moquet, J. S., Noriega, L., Lavado, W.,  
1067 Pombosa, R., and Vauchel, P.: Climatic control on eastern Andean denudation rates (Central  
1068 Cordillera from Ecuador to Bolivia), *J. S. Am. Earth Sci.*, 44, 85-93,  
1069 10.1016/j.jsames.2012.12.010, 2013.

1070 Ponton, C., West, A. J., Feakins, S. J., and Galy, V.: Leaf wax biomarkers in transit record river  
1071 catchment composition, *Geophys. Res. Lett.*, 41, 6420-6427, 10.1002/2014GL061328, 2014.

1072 Quesada, C. A., Lloyd, J., Schwarz, M., Patiño, S., Baker, T. R., Czimczik, C., Fyllas, N. M., Martinelli, L.,  
1073 Nardoto, G. B., Schmerler, J., Santos, A. J. B., Hodnett, M. G., Herrera, R., Luizão, F. J., Arneeth,  
1074 A., Lloyd, G., Dezzio, N., Hilke, I., Kuhlmann, I., Raessler, M., Brand, W. A., Geilmann, H.,  
1075 Moraes Filho, J. O., Carvalho, F. P., Araujo Filho, R. N., Chaves, J. E., Cruz Junior, O. F.,  
1076 Pimentel, T. P., and Paiva, R.: Variations in chemical and physical properties of Amazon  
1077 forest soils in relation to their genesis, *Biogeosciences*, 5, 1515 - 1541, 10.5194/bg-7-1515-  
1078 2010, 2010.

1079 Raich, J. W., Russell, A. E., Kitayama, K., Parton, W. J., and Vitousek, P. M.: Temperature influences  
1080 carbon accumulation in moist tropical forests, *Ecology*, 87, 76-87, 10.1890/05-0023, 2006.

1081 Ramos Scharrón, C. E., Castellanos, E. J., and Restrepo, C.: The transfer of modern organic carbon by  
1082 landslide activity in tropical montane ecosystems, *J. Geophys. Res.-Biogeo.*, 117, G03016,  
1083 10.1029/2011JG001838, 2012.

1084 Rao, Y.: Variation in plant carbon and nitrogen isotopes along an altitudinal gradient in the Peruvian  
1085 Andes, *B.Sc.*, Department of Earth Sciences, Durham University, Durham, 60 pp., 2011.

1086 Restrepo, C., Vitousek, P., and Neville, P.: Landslides significantly alter land cover and the  
1087 distribution of biomass: an example from the Ninole ridges of Hawai'i, *Plant Ecol.*, 166, 131-  
1088 143, 10.1023/A:1023225419111, 2003.

1089 Restrepo, C., and Alvarez, N.: Landslides and their contribution to land-cover change in the  
1090 mountains of Mexico and Central America, *Biotropica*, 38, 446-457, 10.1111/j.1744-  
1091 7429.2006.00178.x, 2006.

1092 Restrepo, C., Walker, L. R., Shiels, A. B., Bussmann, R., Claessens, L., Fisch, S., Lozano, P., Negi, G.,  
1093 Paolini, L., and Poveda, G.: Landsliding and its multiscale influence on mountainscapes,  
1094 *Bioscience*, 59, 685-698, 10.1525/bio.2009.59.8.10, 2009.

1095 Roering, J. J., Kirchner, J. W., and Dietrich, W. E.: Characterizing structural and lithologic controls on  
1096 deep-seated landsliding: Implications for topographic relief and landscape evolution in the  
1097 Oregon Coast Range, USA, *Geol. Soc. Am. Bull.*, 117, 654-668, 10.1130/B25567.1, 2005.

1098 Roering, J. J., Mackey, B. H., Handwerger, A. L., Booth, A. M., Schmidt, D. A., Bennett, G. L., and  
1099 Cerovski-Darriau, C.: Beyond the angle of repose: A review and synthesis of landslide  
1100 processes in response to rapid uplift, Eel River, Northern California, *Geomorphology*, 236,  
1101 109-131, 10.1016/j.geomorph.2015.02.013, 2015.

1102 Rohrmann, A., Strecker, M. R., Bookhagen, B., Mulch, A., Sachse, D., Pingel, H., Alonso, R. N.,  
1103 Schildgen, T. F., and Montero, C.: Can stable isotopes ride out the storms? The role of  
1104 convection for water isotopes in models, records, and paleoaltimetry studies in the central  
1105 Andes, *Earth Planet Sc. Lett.*, 407, 187-195, 10.1016/j.epsl.2014.09.021, 2014.

1106 Saatchi, S. S., Houghton, R. A., Dos Santos Alvalá, R. C., Soares, J. V., and Yu, Y.: Distribution of  
1107 aboveground live biomass in the Amazon basin, *Glob. Change Biol.*, 13, 816-837,  
1108 10.1111/j.1365-2486.2007.01323.x, 2007.

1109 Saatchi, S. S., Harris, N. L., Brown, S., Lefsky, M., Mitchard, E. T., Salas, W., Zutta, B. R., Buermann,  
1110 W., Lewis, S. L., and Hagen, S.: Benchmark map of forest carbon stocks in tropical regions  
1111 across three continents, *P. Natl. Acad. Sci. USA*, 108, 9899-9904, 10.1073/pnas.1019576108,  
1112 2011.

1113 Safran, E. B., Bierman, P. R., Aalto, R., Dunne, T., Whipple, K. X., and Caffee, M.: Erosion rates driven  
1114 by channel network incision in the Bolivian Andes, *Earth Surf. Proc. Land.*, 30, 1007-1024,  
1115 10.1002/esp.1259, 2005.

1116 Salazar, L., Homeier, J., Kessler, M., Abrahamczyk, S., Lehnert, M., Krömer, T., and Kluge, J.: Diversity  
1117 patterns of ferns along elevational gradients in Andean tropical forests, *Plant Ecol. Divers.*, 8,  
1118 13-24, 10.1080/17550874.2013.843036, 2015.

1119 Schmidt, K. M., and Montgomery, D. R.: Limits to relief, *Science*, 270, 617-620,  
1120 10.1126/science.270.5236.617, 1995.

1121 Sébrier, M., Mercier, J. L., Mégard, F., Laubacher, G., and Carey-Gailhardis, E.: Quaternary normal  
1122 and reverse faulting and the state of stress in the central Andes of south Peru, *Tectonics*, 4,  
1123 739-780, 10.1029/TC004i007p00739, 1985.

1124 Selby, M.: *Hillslope materials and processes*, Oxford University Press, Oxford, UK, 289 pp., 1993.

1125 Stallard, R. F.: *River chemistry, geology, geomorphology, and soils in the Amazon and Orinoco Basins,*  
1126 *The chemistry of weathering*, Rodez, France, 293-316, 1985.

1127 Stallard, R. F.: *Terrestrial sedimentation and the carbon cycle: Coupling weathering and erosion to*  
1128 *carbon burial*, *Global Biogeochem. Cy.*, 12, 231-257, 10.1029/98gb00741, 1998.

1129 Stark, C. P., and Hovius, N.: The characterization of landslide size distributions, *Geophys. Res. Lett.*,  
1130 28, 1091-1094, 10.1029/2000GL008527, 2001.

1131 Stock, J., and Dietrich, W. E.: Valley incision by debris flows: Evidence of a topographic signature,  
1132 *Water Resour. Res.*, 39, 1-24, 10.1029/2001WR001057, 2003.

1133 Stoyan, R.: *Aktivität, Ursachen und Klassifikation der Rutschungen in San Francisco/Süd Ecuador,*  
1134 *Diploma*, University of Erlangen-Nuremberg, Erlangen, Germany, 2000.

1135 Strecker, M. R., Alonso, R. N., Bookhagen, B., Carrapa, B., Hilley, G. E., Sobel, E. R., and Trauth, M. H.:  
1136 Tectonics and climate of the Southern Central Andes, *Annu. Rev. Earth Pl. Sc.*, 35, 747-787,  
1137 10.1146/annurev.earth.35.031306.140158, 2007.

1138 Tavera, H., and Buforn, E.: Source mechanism of earthquakes in Perú, *J. Seismol.*, 5, 519-540,  
1139 10.1023/A:1012027430555, 2001.

1140 Terzaghi, K.: Mechanism of landslides, Harvard University, Department of Engineering, Cambridge,  
1141 Massachusetts, USA, 41 pp., 1951.

1142 USGS: Earthquakes v3.6, 2013-07-02, USGS, <http://earthquake.usgs.gov/earthquakes/map/>, access:  
1143 02/07/2013, 2013a.

1144 USGS: Landsat Processing Details, United States Geological Survey, U.S. Department of the Interior,  
1145 [http://landsat.usgs.gov/Landsat\\_Processing\\_Details.php](http://landsat.usgs.gov/Landsat_Processing_Details.php), access: 16/7/2013, 2013b.

1146 Vargas Vilchez, L., and Hipolito Romero, A.: Geología de los cuadrángulos de Río Pinquén, Pilcopata y  
1147 Chontachaca. Hojas: 25-t, 26-t y 27-t, Instituto Geológica Nacional, Lima, Peru, 1998.

1148 Walker, L. R., Zarin, D. J., Fetcher, N., Myster, R. W., and Johnson, A. H.: Ecosystem development and  
1149 plant succession on landslides in the Caribbean, *Biotropica*, 28, 566-576, 10.2307/2389097,  
1150 1996.

1151 Walker, L. R., Shiels, A. B., Bellingham, P. J., Sparrow, A. D., Fetcher, N., Landau, F. H., and Lodge, D.  
1152 J.: Changes in abiotic influences on seed plants and ferns during 18 years of primary  
1153 succession on Puerto Rican landslides, *J. Ecol.*, 101, 650-661, 10.1111/1365-2745.12071,  
1154 2013.

1155 Wang, G., and Sassa, K.: Pore-pressure generation and movement of rainfall-induced landslides:  
1156 effects of grain size and fine-particle content, *Eng. Geol.*, 69, 109-125, 10.1016/S0013-  
1157 7952(02)00268-5, 2003.

1158 Wang, J., Jin, Z., Hilton, R. G., Zhang, F., Densmore, A. L., Li, G., and West, A. J.: Controls on fluvial  
1159 evacuation of sediment from earthquake-triggered landslides, *Geology*, 43, 115-118,  
1160 10.1130/G36157.1, 2015.

1161 West, A. J., Lin, C. W., Lin, T. C., Hilton, R. G., Liu, S. H., Chang, C. T., Lin, K. C., Galy, A., Sparkes, R. B.,  
1162 and Hovius, N.: Mobilization and transport of coarse woody debris to the oceans triggered  
1163 by an extreme tropical storm, *Limnol. Oceanogr.*, 56, 77-85, 10.4319/lo.2011.56.1.0077,  
1164 2011.

1165 Whipple, K. X.: Fluvial landscape response time: How plausible is steady-state denudation?, *Am. J.*  
1166 *Sci.*, 301, 313-325, 10.2475/ajs.301.4-5.313, 2001.

1167 Whipple, K. X.: Bedrock rivers and the geomorphology of active orogens, *Annu. Rev. Earth Pl. Sc.*, 32,  
1168 151-185, 10.1146/annurev.earth.32.101802.120356, 2004.

1169 Whipple, K. X., and Gasparini, N. M.: Tectonic control of topography, rainfall patterns, and erosion  
1170 during rapid post-12 Ma uplift of the Bolivian Andes, *Lithosphere*, 6, 251-268,  
1171 10.1130/l325.1, 2014.

1172 Wittmann, H., von Blanckenburg, F., Guyot, J. L., Maurice, L., and Kubik, P.: From source to sink:  
1173 Preserving the cosmogenic <sup>10</sup>Be-derived denudation rate signal of the Bolivian Andes in  
1174 sediment of the Beni and Mamoré foreland basins, *Earth Planet Sc. Lett.*, 288, 463-474,  
1175 10.1016/j.epsl.2009.10.008, 2009.

1176 Wohl, E., and Ogden, F. L.: Organic carbon export in the form of wood during an extreme tropical  
1177 storm, Upper Rio Chagres, Panama, *Earth Surf. Proc. Land.*, 38, 1407-1416,  
1178 10.1002/esp.3389, 2013.

1179 Wolman, M. G., and Miller, J. P.: Magnitude and frequency of forces in geomorphic processes, *J.*  
1180 *Geol.*, 68, 54-74, 1960.

1181 Yang, R., Willett, S. D., and Goren, L.: In situ low-relief landscape formation as a result of river  
1182 network disruption, *Nature*, 520, 526-529, 10.1038/nature14354, 2015.

1183 Yoo, K., Amundson, R., Heimsath, A. M., and Dietrich, W. E.: Erosion of upland hillslope soil organic  
1184 carbon: Coupling field measurements with a sediment transport model, *Global Biogeochem.*  
1185 *Cy.*, 19, GB3003, 10.1029/2004GB002271, 2005.

1186 Zhang, W., and Montgomery, D. R.: Digital elevation model grid size, landscape representation,  
1187 Water Resour. Res., 30, 1019-1028, 1994.  
1188 Zimmermann, M., Meir, P., Bird, M. I., Malhi, Y., and Ccahuana, A. J. Q.: Climate dependence of  
1189 heterotrophic soil respiration from a soil-translocation experiment along a 3000 m tropical  
1190 forest altitudinal gradient, Eur. J. Soil Sci., 60, 895-906, 10.1111/j.1365-2389.2009.01175.x,  
1191 2009.

1192

1193

1194

Equation	Number of plots	R <sup>2</sup>	P	Source of data
Soil = 4.01±4.64 x Elevation + 16665.22±11753.06	11 (with 6 to 51 subplots)	0.08	0.19	This study
AGLB = -1.16±0.65 x Elevation + 8553.71±1644.36	13	0.22	0.10	This study
BGLB = -0.22±0.13 x Elevation + 2237.09±280.18	6	0.43	0.16	(Girardin et al., 2010)

AGLB = Above ground living biomass (includes tree stems)  
BGLB = Below ground living biomass (includes fine and coarse roots)  
Regressions used to gain a general understanding of C stocks with elevation and significance of the relationship with elevation is not relevant.

1195

1196

1197

Table 2: Valley-wide landslide stripped organic carbon ( $\text{tC km}^{-2} \text{yr}^{-1}$ ).

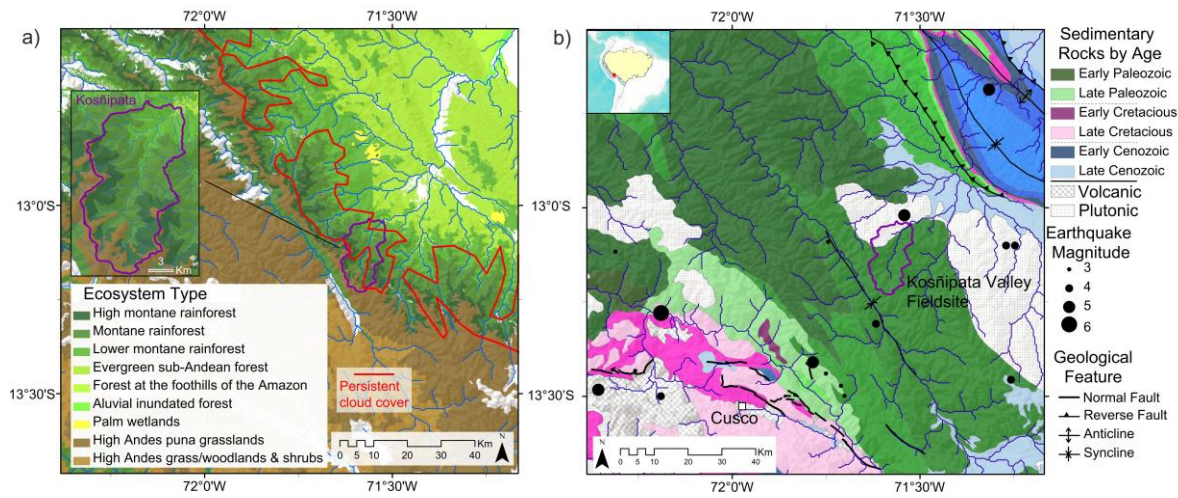
	1988 to 2012	Without 2010	2010
Total	$25.8 \pm 3.6$	$19.1 \pm 3.0$	$6.8 \pm 1.2$
Soil	$20.1 \pm 3.5$	$15.1 \pm 2.9$	$5.0 \pm 1.2$
Vegetation	$5.7 \pm 0.8$	$4.0 \pm 0.7$	$1.7 \pm 0.2$

1198

1199

1200  
1201

## Figures

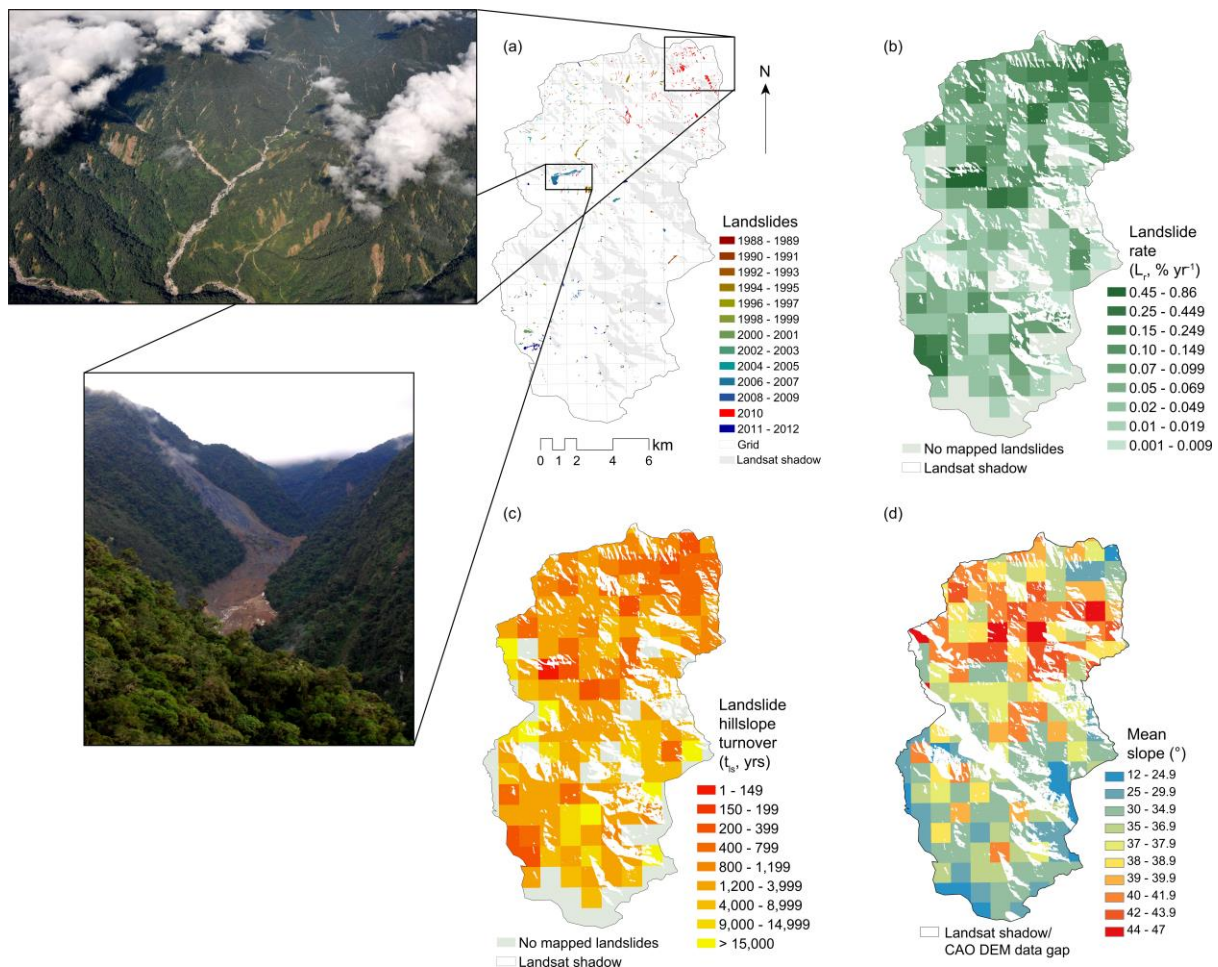


1202

1203 Figure 1: Maps of the study region. (a) Ecosystem types in the eastern Andes of Peru (Consbio, 2011).  
1204 Bare areas are cities, agriculture, glaciers and riverbed, with the Kosñipata study catchment magnified  
1205 in the inset. Areas delimited by red polygons are regions of > 75% annual cloud cover (Halladay et  
1206 al., 2012). (b) Georectified geological map (INGEMMET, 2013; Vargas Vilchez and Hipolito  
1207 Romero, 1998; Carlotto Caillaux et al., 1996; Mendivil Echevarría and Dávila Manrique, 1994);  
1208 sedimentary rocks are on a scale ranging from dark to light colour within each era. Active faults  
1209 (Cabrera et al., 1991; Sébrier et al., 1985) and documented earthquakes since 1975 (USGS, 2013a) are  
1210 shown.

1211

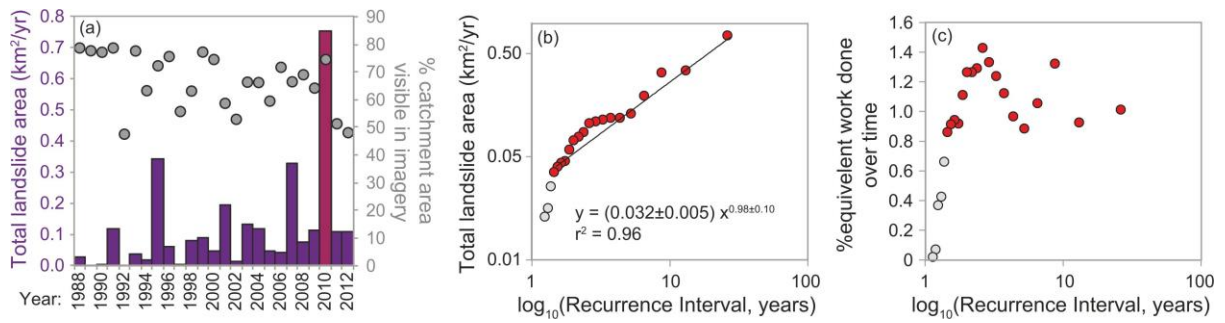
1212



1213

1214 Figure 2: (a) Landslides over the 25-year study period mapped from Landsat satellite images with  
 1215 annual resolution, with Landsat topographic shadow regions in light grey. Photographs of the 2010  
 1216 landslides (upper) taken by Gregory P. Asner from the Carnegie Airbone Observatory (CAO) in 2013,  
 1217 and of the largest landslide in the study in 2007 (lower) taken by William Farfan-Rios from the  
 1218 ground in 2011. (b) Landslide rates ( $R_{ls}$ , %  $yr^{-1}$ ) calculated by 1  $km^2$  grid cell. (c) Hillslope turnover  
 1219 ( $t_{ls}$ , yr) rates calculated as the time for landslides, at the current measured rate ( $R_{ls}$ ), to impact 100% of  
 1220 each cell area. (d) Catchment slopes calculated over a 1  $km^2$  grid for the visible portion of the study  
 1221 area using the CAO DEM with 3m x 3m resolution.

1222

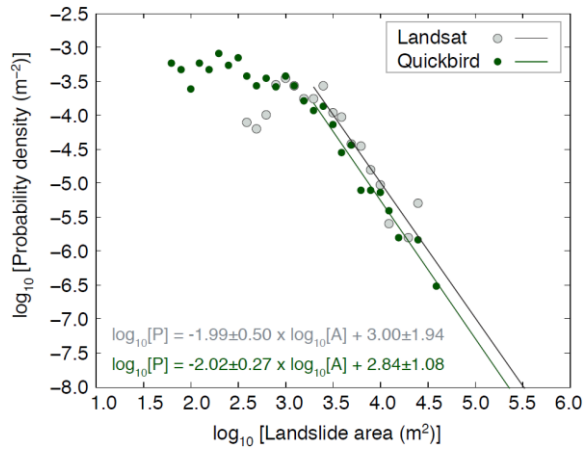


1223

1224 Figure 3: (a) Total area of landslides occurring each year in the dataset from this study, along with the  
 1225 % area visible in the images used for each year. (b) Magnitude-frequency relationship for landslide  
 1226 areas mapped in each year; red points are included in the regression while grey point are excluded  
 1227 since these lowest-magnitude years depart from the linear relationship. (c) Estimate of integrated  
 1228 work done by repeated events characteristic of given return times (see main text). Landslide area  
 1229 mapped in 2010 was significantly higher than any other year because of landslides triggered by the  
 1230 large storm in March 2010, but above a threshold magnitude, the integrated long-term landslide area  
 1231 triggered by repeated events of smaller magnitude is similar to that done by larger, rarer events in this  
 1232 dataset, as revealed by the similar % of equivalent work done for years across a wide range of inferred  
 1233 recurrence interval.

1234

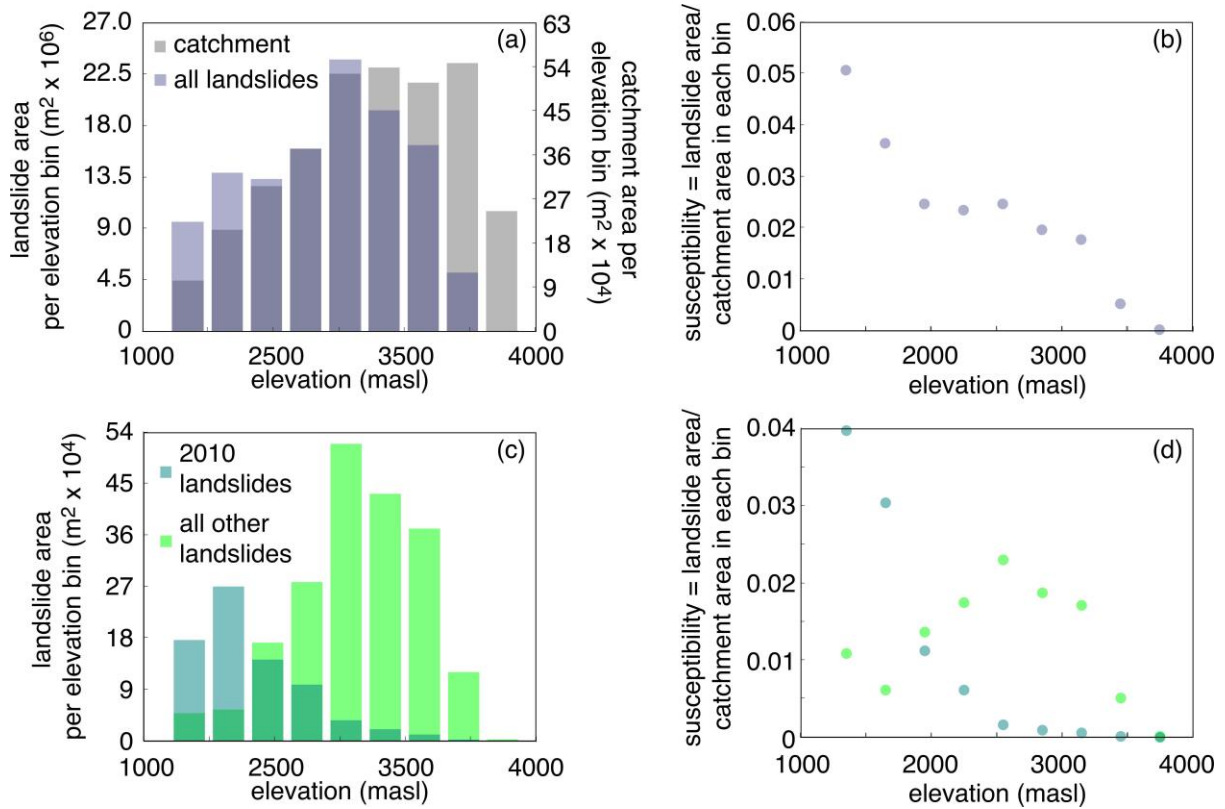
1235



1236

1237 Figure 4: Landslide area-frequency diagram for all landslides mapped from 1988 to 2005 in a region  
 1238 of the Landsat image that overlapped with a Quickbird image from 2005, and for all landslides present  
 1239 in the Landsat visible region of the Quickbird image. The higher frequency of small landslides in the  
 1240 Quickbird inventory can be explained by the higher resolution of this image (2.4 m x 2.4 m, compared  
 1241 to 30 m x 30 m for Landsat). The power law tails of the two inventories are similar.

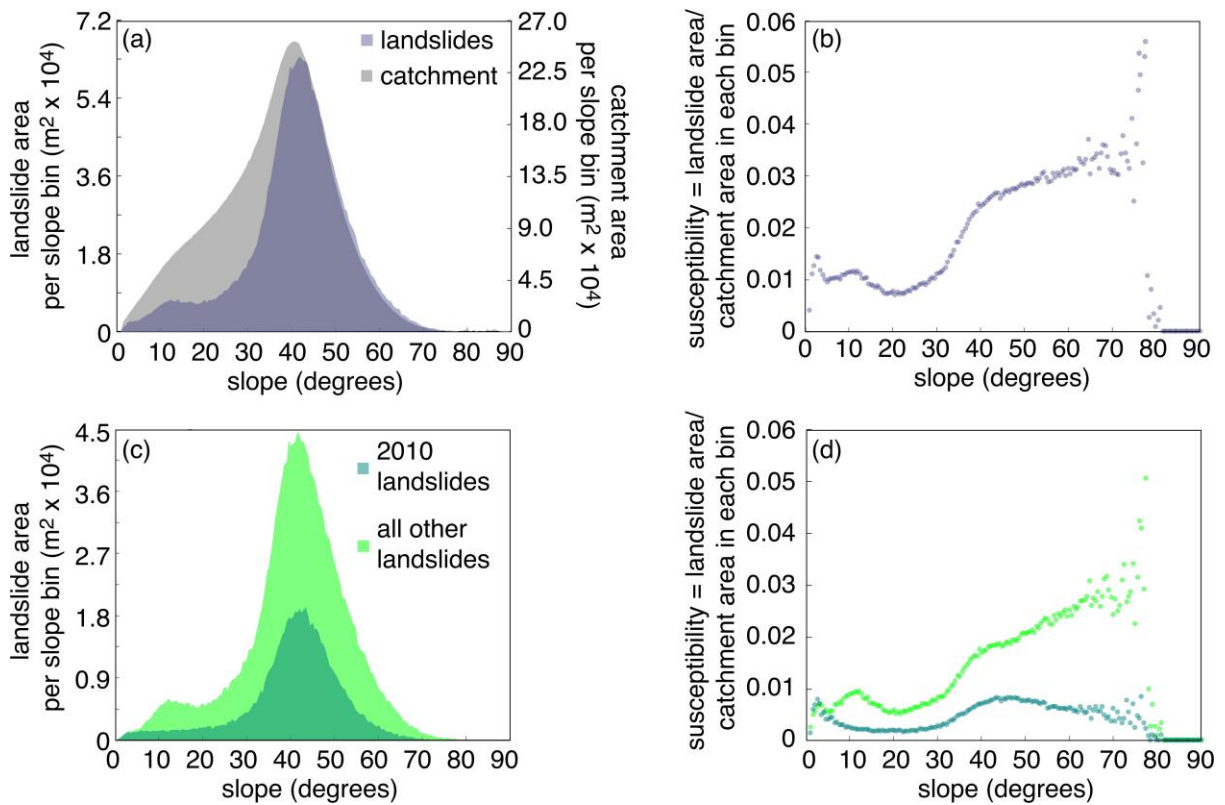
1242



1243

1244 Figure 5: Histograms of catchment and landslide areas by elevation bins of 300 m: (a) all landslides in  
 1245 the 25-year dataset; (c) separating landslides occurring during 2010, associated with the large storm in  
 1246 March 2010, from those in the rest of the dataset. (b) and (d) Corresponding calculation of landslide  
 1247 susceptibility, calculated as the area of landslides within each bin divided by the total visible area in  
 1248 the Landsat images used for mapping.

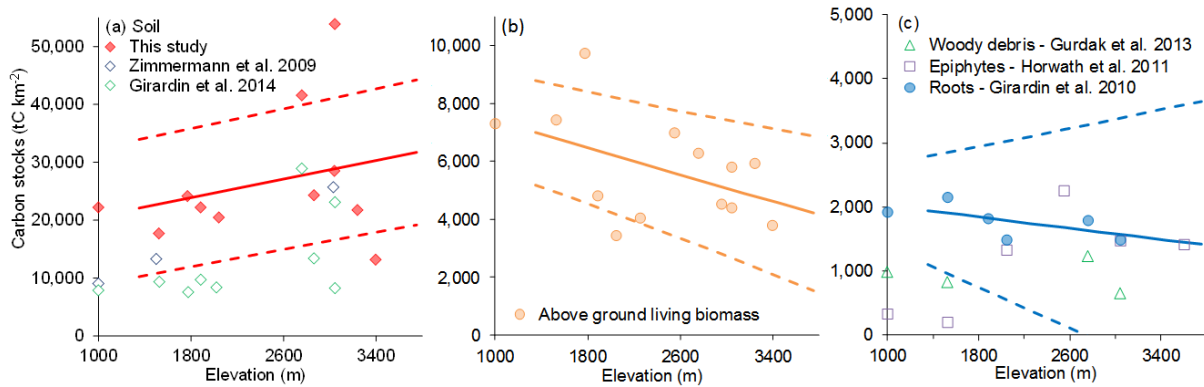
1249



1250

1251 Figure 6: Histograms of catchment and landslide areas by slope bins of  $1^\circ$ : (a) all landslides in the 25-  
 1252 year dataset; (c) separating landslides occurring during 2010, associated with the large storm in March  
 1253 2010, from those in the rest of the dataset. (b) and (d) Corresponding calculation of landslide  
 1254 susceptibility, calculated as the area of landslides within each bin divided by the total visible area in  
 1255 the Landsat images used for mapping.

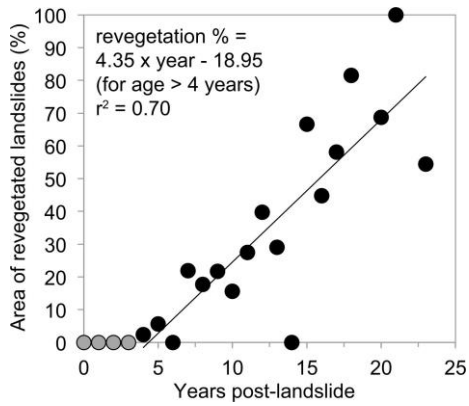
1256



1257

1258 Figure 7: Soil and vegetation carbon stocks ( $\text{tC km}^{-2}$ ) as a function of elevation for the tropical  
 1259 montane forest of Kosñipata Valley, in the eastern Andes of Peru (Girardin et al., 2014a; Gurdak et  
 1260 al., 2014; Horwath, 2011; Girardin et al., 2010; Zimmermann et al., 2009). Linear regressions  
 1261 generated from available carbon stock data ( $\text{tC km}^{-2}$ ) from the Kosñipata Valley for a) soil carbon  
 1262 stocks (red diamonds only; see Figure S1 and section 3.3.2. comparing the soil data with other  
 1263 datasets), b) above ground living biomass, and c) root biomass (Table 1). c) Woody debris, and  
 1264 epiphytes are shown for reference.

1265



1266

1267

Figure 8: Landslide revegetation time as percent area recovered by 2011, evaluated from a

1268

WorldView-2 pan-sharpened satellite image at 2 m x 2 m resolution. Each data point represents the

1269

landslides from a single year during the study period (black and grey circles; n = 23). Landslides

1270

occurring at least 4 years prior to 2011 (black circles) were used to calculate the best fit (area of

1271

revegetated landslides (%) =  $4.351 \pm 0.719 \times \text{year of landslide origin prior to 2011} - 18.953 \pm 9.974$ ,

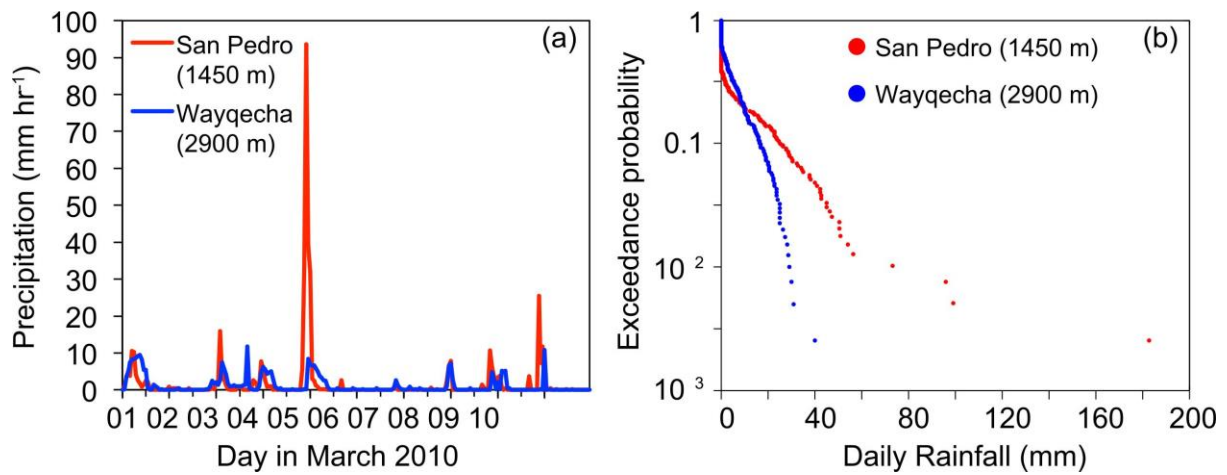
1272

where the mean estimated time for 100% revegetation of all the landslides of a given year is  $27 \pm 8$  yrs

1273

( $r^2 = 0.7$ ,  $n = 18$ ,  $p < 0.0001$ ).

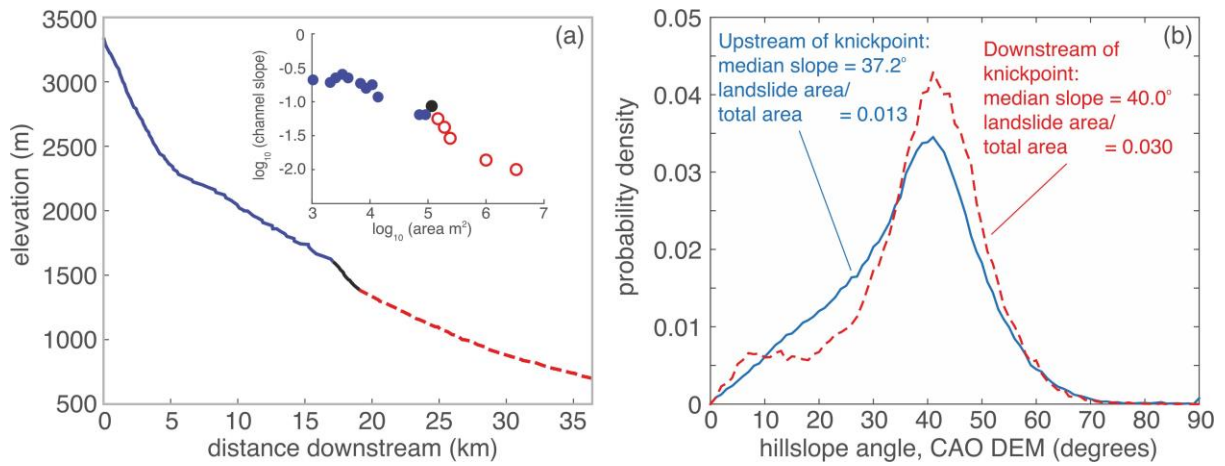
1274



1275

1276 Figure 9: (a) Precipitation during the March 2010 storm in the Kosñipata Valley at two stations, one at  
 1277 high elevation (Wayqecha plot, 2900 m), where storm precipitation was low, and another at low  
 1278 elevations (San Pedro, 1450 m; Clark et al., 2014; ACCA, 2012), where precipitation was high and  
 1279 where occurrence of storm-triggered landslides was also high (e.g., Fig. 5c). (b) Magnitude-frequency  
 1280 analysis of precipitation over multiple years at the two stations shown in (a), demonstrating that the  
 1281 low elevations in the Kosñipata study catchment are generally characterized by more low-frequency,  
 1282 high-magnitude precipitation events.

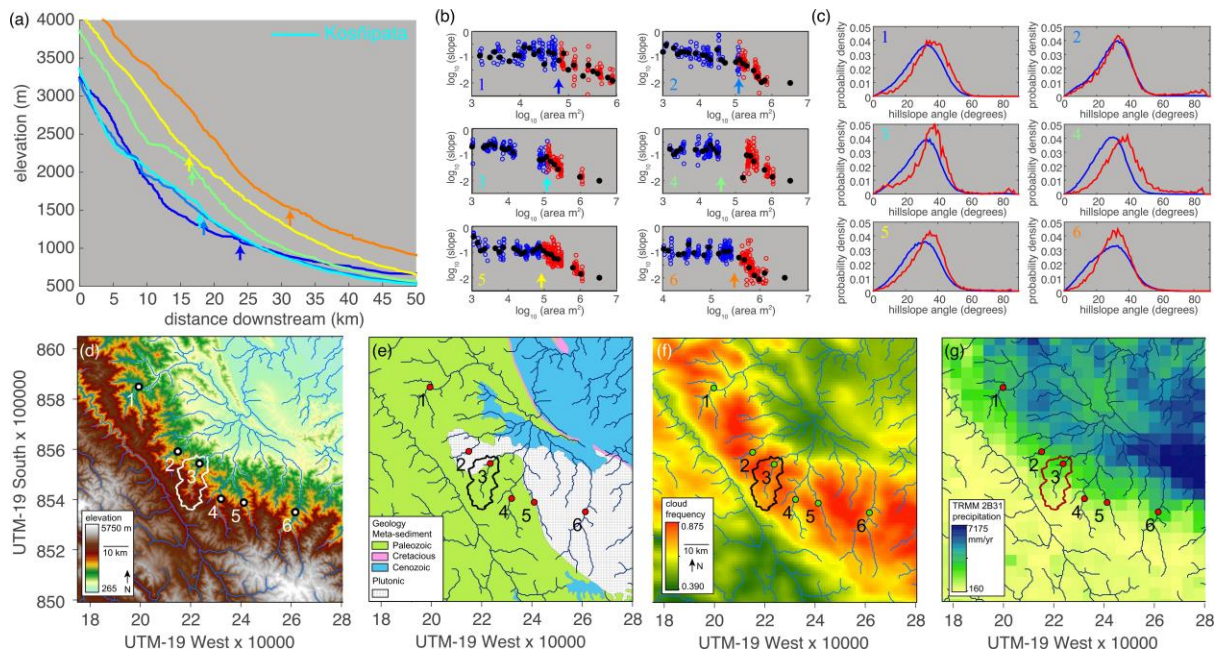
1283



1284

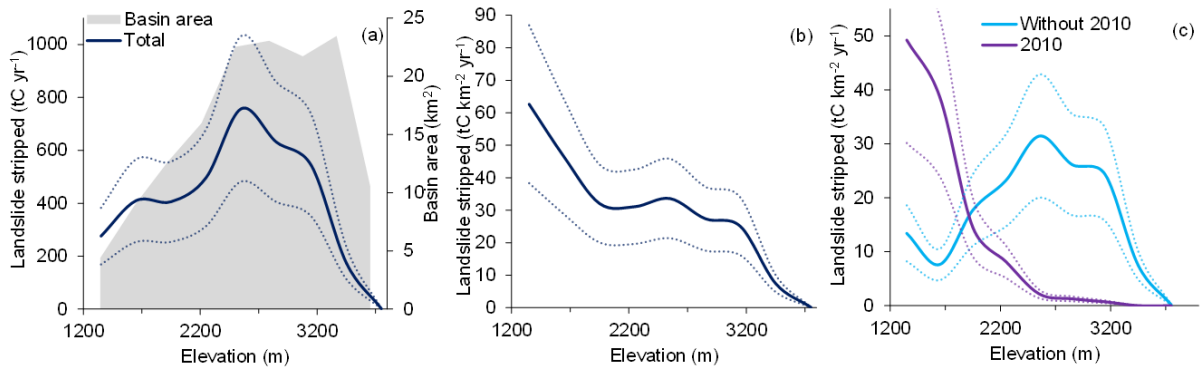
1285 Figure 10: (a) Longitudinal profile along the Kosñipata river channel, with a prominent vertical step  
 1286 knickpoint corresponding to (inset) a transition in the plot between channel slope and upstream  
 1287 contributing area, calculated following Moon et al. (2011). (b) Probability density of hillslope angles  
 1288 (from 3 m x 3 m CAO DEM) upstream and downstream of the morphological transition in the  
 1289 channel, along with median hillslope angles in each region and landslide susceptibility over the 25-  
 1290 year study period.

1291



1292

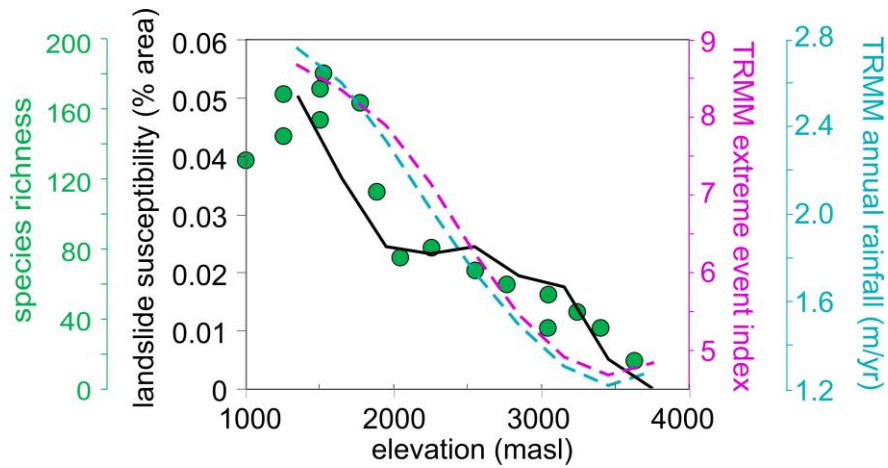
1293 Figure 11: (a-c) Analysis of river profiles analogous to those in Fig. 10 (shown here as River #3, in  
 1294 cyan), for rivers throughout the Alto Madre de Dios region (d). In (b), data are binned by upstream  
 1295 area and means are shown by black circles. Arrows in (a) refer to locations along the profile of  
 1296 observed transition in the area-slope plots (b). In (c), hillslope angles (from STRM DEM) are grouped  
 1297 by upstream (blue) and downstream (red) of this transition. Transition locations are displayed as dots  
 1298 in (d-g), which show regional elevation (Farr et al., 2007) (d), geology (INGEMMET, 2013) (e),  
 1299 Modis cloud frequency (Halladay et al., 2012) (f), and TRMM 2B31 annual precipitation (Bookhagen,  
 1300 2013) (g).



1301

1302 Figure 12: (a) Total mobilisation of organic carbon by landslides (tC yr<sup>-1</sup>) and (b) area-normalised  
 1303 mobilisation of organic carbon (tC km<sup>-2</sup> yr<sup>-1</sup>) over the altitudinal gradient divided into 300 m elevation  
 1304 bins contributed by the sum of soil and vegetation (total, navy line), with errors as dotted lines.  
 1305 Landslide susceptibility is highest at low elevations so the yield is highest there (b), but the total flux  
 1306 due to landslides is dominated by mid-elevations that comprise the majority of basin area (a). (c)  
 1307 Separation of landslide-mobilised organic carbon (tC km<sup>-2</sup> yr<sup>-1</sup>) due to the 2010 rain storm event from  
 1308 the remaining years as a function of elevation.

1309



1310

1311 Figure 13: Plots of landslide susceptibility, TRMM-based precipitation (both total annual precipitation  
 1312 and TRMM extreme event index) (Bookhagen, 2013), and species richness, as a function of elevation  
 1313 within the Kosñipata Valley. Note that absolute values of 2B31 TRMM annual precipitation are not  
 1314 accurate without calibration to meteorological station data (cf. Clark et al., 2014) but spatial patterns  
 1315 may be representative. Climatology, landslide occurrence, and species richness all generally increase  
 1316 from high to low elevations within the Kosñipata Valley, although landslide susceptibility and species  
 1317 richness show a discontinuous trend with elevation while TRMM-based climatology is more  
 1318 continuous.